NTNU

Norwegian University of
Science and Technology

Assembly and Testing of Superconducting Field Winding

Morten Ellingsen Paulsen

Master of Energy and Environmental Engineering
Submission date: June 2016
Supervisor: Arne Nysveen, ELKRAFT
Co-supervisor: Niklas Magnusson, SINTEF Energi

Norwegian University of Science and Technology
Department of Electric Power Engineering

NORGES TEKNISK-NATURVITENSKAPELIGE UNIVERSITET

NTNU

M A S T E R O P P G A V E

Kandidatens navn:	Morten Ellingsen Paulsen
Fag:	**ELKRAFTTEKNIKK**
Oppgavens tittel (norsk):	Sammenstilling og testing av MgB_2 superledende feltvikling
Oppgavens tittel (engelsk):	Assembly and testing of a MgB_2 superconducting field winding

Oppgavens tekst:
Superconducting rotor windings are considered for large off-shore wind turbine generators to reduce weight, size and cost. Superconductors carry DC currents loss-free when cooled down to low temperatures and their current densities are about 100 times higher than in copper conductors. Within an EU-project, 10 pcs. of 2-layer superconducting coils have been made at SINTEF Energy Research during 2014 and 2015. The coil is shaped like a race track, and is 1 m long and half a meter wide.

This master thesis concerns assembly of the previously made winding disks into a complete winding using the soldering process developed in the project work by the candidate autumn 2015.

More specifically the work shall focus on:

- Assembly of all previously fabricated winding discs to a complete field winding
- Assembly of the winding into the cooling and mechanical supporting jig including cooling of the coil joints
- Mounting of measurement leads for voltage measurement to confirm superconductivity and joint quality.
- Assembly of the complete field winding into the cryostat vessel
- Cooling of the field winding to achieve superconductivity
- Confirm superconductivity by measurements

Further details of the work are to be discussed with the supervisors during the project period.

Oppgaven gitt:	15. januar 2016
Oppgaven revidert:	19. mai 2016
Besvarelsen leveres innen:	24. juni 2016
Besvarelsen levert:	24. juni 2016
Utført ved (institusjon, bedrift):	Inst. for elkraftteknikk/NTNU
Kandidatens veileder:	Niklas Magnusson, SINTEF Energy
Faglærer:	Professor Arne Nysveen

Trondheim, 19. mai 2016

Arne Nysveen
Faglærer

Preface

This master thesis is a study carried out for the Department of Electric Power Engineering at the Norwegian University of Science and Technology during spring semester 2016.

The subject is proposed by SINTEF Energy Research and is a part of an European project called INNWIND.EU. The overall objective of the INNWIND.EU project is to find new and innovating solutions for bigger offshore wind turbines with power ratings higher than 10MW.

I would like to thank my supervisors Professor Arne Nysveen at the Department of Electric Power Engineering, NTNU and Niklas Magnusson from SINTEF Energy Research, for their involvement during the project.

I would also show my gratitude to the workers at the NTNU workshop for great assistance and help during the project. Their involvement resulted in good solutions of every practical challenges.

Trondheim, June 24. 2016

Morten Ellingsen Paulsen

Abstract

Superconducting rotor windings are considered for large offshore wind turbines to reduce weight, size and cost. The European project INNWIND.EU utilize various national projects in different European countries to accelerate the development of innovations that can help realize larger wind turbines. SINTEF Energy Research is one of the organizations that are involved in this project by designing, building and testing a superconducting rotor field winding. This could potentially reduce weight, volume and cost of future wind turbines.

This master thesis describes the method and steps that were done to complete a superconducting field winding and how it was tested.

Ten MgB_2 double pancake coils were glued together with a thermally conductive epoxy on a thermal interface. The coils were joined electrically by a validated procedure that makes low resistance joints by using a custom made soldering tool. BSCCO high temperature superconductors were soldered at each end of the field winding to lead the current from the high temperature stage of the cryostat to the field winding. A mechanical support placed around the field winding was designed to withstand the magnetic forces acting on the field winding during testing.

The field winding was placed in a cryostat and cooled down to 17.7°K for testing. Seven out of ten coils were proved to be superconductive. Coil 1, 6, 10 and the BSCCO HTS were not superconductive as a voltage was measured when a current was flowing through the field winding. The quality of the joints was validated by measuring the voltage over each joint and calculating the resistance. The average resistance of the joints was 40nΩ where the highest resistance was 110nΩ. 15mW of heat would be dissipated in the joints when testing with a current of 200A. The inductance of the field winding was found to be 4.6H.

Sammendrag

Superledende rotorviklingene kan utvikle offshore vindturbiner ved å redusere vekt, størrelse og pris. Det europeiske prosjektet INNWIND.EU utnytter ulike nasjonale prosjekter i ulike europeiske land for å akselerere utviklingen av innovasjoner som kan bidra til å realisere større vindturbiner. SINTEF Energi er en av organisasjonene som er involvert i dette prosjektet ved å designe, bygge og teste en superledende rotor vikling. Dette kan potensielt redusere vekt, volum og kostnad for fremtidige vindturbiner.

Denne masteroppgaven beskriver metoden og fremgangsmåten som ble gjort for å fullføre en superledende feltvikling og hvordan den ble testet.

Ti MgB_2 spoler ble limt sammen med en termisk ledende epoksy og holdt på plass av to kopperplater som er koblet til kjølemaskinen. Spolene ble skjøtet elektrisk med en validert prosedyre som gjør at skjøtene får en lav motstand. Dette ble gjort ved hjelp av en spesiallaget loddebolt. BSCCO høytemperatur superledere ble loddet på hver ende av feltviklingen for å lede strømmen fra det høye temperatur stadiet av kryostaten til feltviklingen. En mekanisk støtte var plassert rundt feltvikling og er designet for å motstå de magnetiske krefter som virker på feltviklingen under testing.

Feltviklingen ble plassert i en cryostat og avkjølt til 17,7 °K for testing. Syv av ti spoler viste seg å være superledende. Spole 1, 6, 10 og BSCCO HTS ble ikke superledende fordi en spenning ble målt over de når en strøm gikk gjennom feltviklingen. Kvaliteten av skjøtene ble validert ved å måle spenningen over hver skjøt slik at man kunne beregne motstanden. Den gjennomsnittlige motstand i skjøtene var 40nΩ, og den høyeste motstanden var 110nΩ. 15mW vil gå tapt som varme i skjøtene når feltviklingen blir testet med en strøm på 200A. Induktansen til feltviklingen ble funnet til å være 4.6H.

Contents

List of Abbreviation

DC	Direct Current
HTS	High temperature superconductors
ICNIRP	International Commission on Non-Ionizing Radiation Protection
LTS	Low temperature superconductors
PIT	Powder in Tube
T_C	Critical Temperature

List of Tables

List of Figures

Chapter 1

Introduction

Further developments in offshore wind are dependent on new technologies to reduce the cost per unit generated energy. One of the technologies that are looked into is the possibility to make rotor windings of superconducting material. Superconducting rotor coils are considered for large offshore wind turbines, with power ratings of 10 MW and beyond, to reduce weight, volume and cost of the turbine. This is possible due to the high current density that is achievable in superconductors when operating in DC-operation. Superconducting field windings can create a magnetic field considerably higher then a conventional copper coil, and the necessary torque can then be realized within a much smaller volume. This volume and weight reduction may have a significant economical value, particularly for wind turbines at depths requiring floating platforms [6].

In the framework of the European project INNWIND.EU, a MgB_2 superconducting rotor coil will be designed, built and tested [6]. The MgB_2 superconductor can carry a current density 25-50 times larger than copper, in the temperature range of 15-20K and a magnetic field of 2T present. This superconductor is chosen due to several factors, such as the critical temperature, magnetic field strength, cost and availability. The MgB_2 conductor is still under development and further cost reduction is possible in the future. The drawback with this technology is the amount of power needed for cooling, and the cost of cryogenic equipment. These aspects need to be included as well in the economical assessment when considering this technology.

As part of the project INNWIND.EU, ten individual coils have been made of MgB_2 superconductor in a previous Master thesis [7], and need to be assembled together to complete a rotor field winding. The sections are shaped like a race track and wounded as a double pancake with epoxy used as electrical insulation between the

turns. This master thesis addresses the procedure and encountered problems during the assembly and testing of the superconducting field winding. The complete field winding is shown in Figure 1.1 and was tested in superconductive state at the end of the project period.

Figure 1.1: The complete field winding assembled with the thermal interface.

Chapter 2

Theory

2.1 Superconductivity

Superconductivity is a phenomenon when the electrical resistivity of the material becomes exactly zero when it is cooled below a critical temperature, T_C. This is a quantum mechanical phenomenon described by different theories that are not discussed in this report. Another remarkable property of a superconductor is that it completely rejects external magnetic field. This is know as the Meissner effect.

2.1.1 History

Superconductivity was discovered in 1911 by Heike Kamerlingh Onnes, a Dutch physicist and professor at the University of Leiden. The discovery of superconductivity was closely connected to Kamerlingh Onnes achievement to be the first person to liquefy helium, using the Hampson-Linde cycle. In 1908, trough several cooling stages, Kamerlingh Onnes was able to lower the temperature to 4.2°K and liquefy helium. This outstanding research made it possible to study the properties of materials at extremely low temperatures. His remarkable achievements were rewarded with the Nobel Prize in Physics in 1913 [8].

With liquid helium Kamerlingh Onnes was now able to cool down materials to extremely low temperatures and study their properties. He was especially interested in the electrical resistivity when the temperature would approach zero Kelvin. This research had never been done before and different hypothesis proposed that the resistivity would reach a minimum or become zero. Kamerlingh Onnes measured resistivity in pure platinum and gold and discovered that the resistivity was highly

dependent on the purity of the metal. The purer the metal was, the lower the resistance became at temperatures lower than 10°K. This discovery led to the testing of mercury, which was easy to make extremely pure through multiple distillations [9]. In 1911 testing of mercury became the discovery of superconductivity as the resistivity dropped to practically zero just below 4.2°K. As Kamerlingh Onnes tested several other materials did he discovered that the phenomenon was not as dependent on purity as first expected. Tests with lead and tin proved that these materials also became superconductive without being particularly pure.

Kammerlingh Onnes did also register another property with superconductivity when he tried to make an electromagnet with superconducting windings. He discovered that with a relatively low magnetic fields would he destroy the superconductivity in the materials. What he discovered was the superconductors dependency on the magnetic field to stay in superconducting state.

Later in the 20th century more elements, alloys and compounds where discovered with superconducting abilities. Unfortunately all of them was only superconductive at extremely low temperatures. A breakthrough was made in 1986 when Alex Müller and Gerog Bednorz discovered superconductivity in a piece of ceramic at 30°K. This was a big surprise as ceramic is usually used as insulators and do not conduct electricity very well in room temperature. The year after, in 1987, the first material entering superconductive state above the boiling point of nitrogen at 77°K was discovered. These superconductors are later know as high-temperature superconductors (HTS). Low temperature superconductors (LTS), on the other hand, need lower temperatures around the boiling point of helium (4°K) [8].

2.1.2 Superconducting Properties and Limitations

The superconductive state is not only dependent on temperature(T_C), Kamerlingh Onnes also discovered a dependence on current density (J_C) and magnetic field (B_C). In order to get into superconductive state must all of the three criteria be fulfilled, creating an interdependent surface called the critical surface. A representation of the critical surface is shown in Figure 2.1, where the operating point of the superconductor needs to be inside the yellow space in order to enter superconducting state.

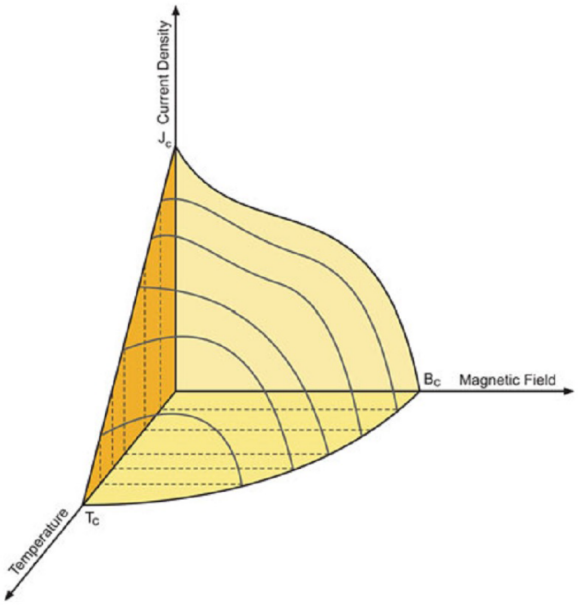

Figure 2.1: Critical surface of a superconductor [2].

In 1933 Walter Meissner and Robert Ochsenfeld discovered what we today call the Meissner effect. A perfect superconductor with zero resistivity implies that the conductor will not sustain an electric field. From Faraday's law;

$$\nabla \times E = -\frac{\partial B}{\partial t} \tag{2.1}$$

$$E = 0 \Rightarrow \frac{\partial B}{\partial t} = 0 \tag{2.2}$$

we can see that if we do not have any electric field, the magnetic flux inside the superconductor should not change and therefore be constant. To prove this, Meissner and Ochsenfeld exposed a superconductor in room temperature with a magnetic field to obtain a constant magnetic flux inside the superconductor. Then they lowered the temperature below the critical temperature, expecting the magnetic flux to be constant inside the superconductor, even when the external magnetic field was removed. This hypothesis proved to be wrong, as Meissner and Ochsenfeld observed an unexpected behavior from the superconductor. When the superconductor entered the superconductive state, the magnetic field inside it became zero. This behavior of repelling the external field and work like a perfect diamagnet is today known as the Meissner effect, and is illustrated in Figure 2.2.

When a magnetic field is applied to a superconductor, currents are induced on the surface producing a magnetic field that cancels out the external field applied. The total magnetic field inside the superconductor is then zero.

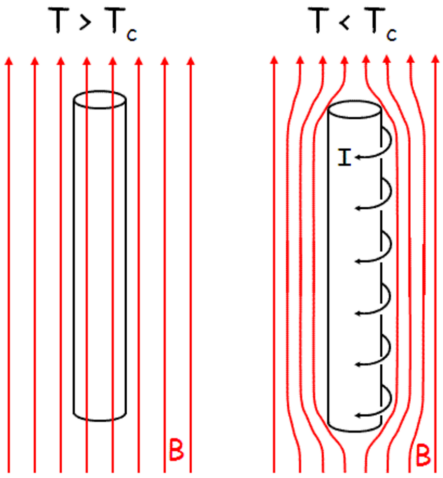

Figure 2.2: Illustration of the magnetic field inside a superconductor over and below critical temperature. The induced current on the surface is illustrated in the superconducting state [3].

2.1.3 Type I and Type II Superconductors

Superconductors are categorized by their abilities to repel external magnetic fields, and are divided in the two categories Type I and Type II. Type I superconductors are perfect diamagnets and repel external magnetic fields completely in superconducting state, as illustrated in the magnetic phase diagram shown in Figure 2.3a. The Type I category is mainly comprised of metals and metalloids which requires low temperatures to become superconductive.

Type II superconductors are perfect diamagnets up to a critical field, B_{C1}, where it starts to allow partial flux penetrations. This state is called the mixed state and is a transition from normal to superconducting state. The flux penetrations are known as vortices and are carrying a specific quantum of flux, Φ_0;

$$\Phi_0 = \frac{h}{2e} = 2.07 \times 10^{-15} \qquad [\text{Wb}] \tag{2.3}$$

Here h is the Planck constant, and e is the elementary charge. The vortices are parallel to the external applied field as seen in Figure 2.4. These flux lines are

arranged in a triangular lattice where each of them are produced by a persistent circulating current in the opposite direction of the screening current. As the external field strength increases beyond the upper critical field, B_{C2}, the entire structure collapses and the material turns back to normal state. The magnetic phase for a Type II superconductor is illustrated in Figure 2.3b. The Type II category of superconductors is comprised of metallic compounds and alloys that usually have higher T_C than Type I superconductors.

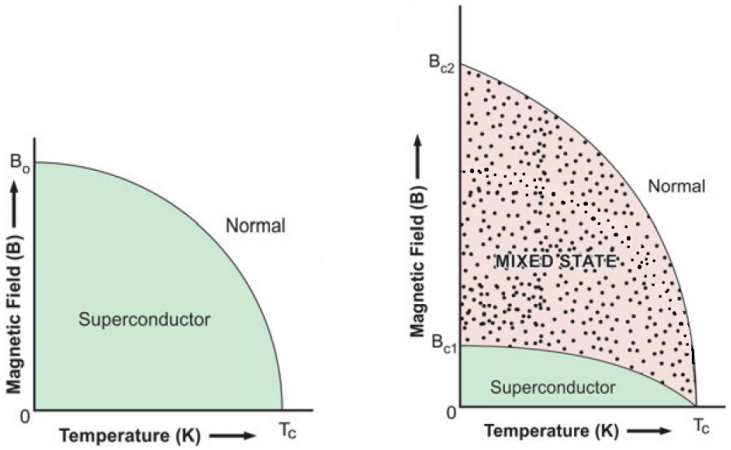

(a) Type I (b) Type II

Figure 2.3: Magnetic phase diagram for Type I and Type II superconductors with respect to temperature and magnetic field [2].

When a large current is carried by a Type II superconductor, the flux lines experience a Lorentz force, F_L, trying to move these lines in the third perpendicular direction as shown in Figure 2.4. The flux lines are held back by the crystal lattice through a pinning force F_P. The Lorentz force is proportional to the current carried by the superconductor, implying a increased Lorentz force when the current is increased. When $F_P \leq F_L$ the vortices starts to move, resulting in an induced voltage and the material gets back to normal state. The current that triggers this is called the critical current I_C, and is also defined as when the electric field reach 1 µV cm^{-1} along the conductor.

The strength of the pinning force, F_P, can be manipulated by introducing defects and impurities into the superconducting material. The defects are placed intelligently to create natural pinning sites such that it gets harder for the vortices to move. This lattice with impurities increases the critical current dramatically, and makes it possible for the superconductor to carry a large current in a high magnetic field. The effect of impurities is illustrated in Figure 2.5, where the current density

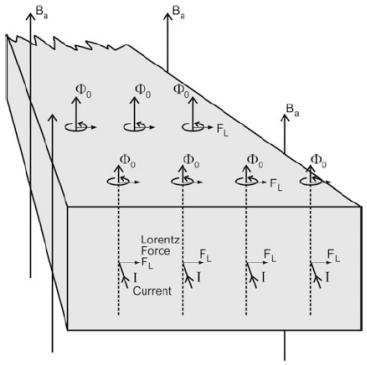

Figure 2.4: Illustration of the vortices in the mixed state, and the force on these when current are present [2].

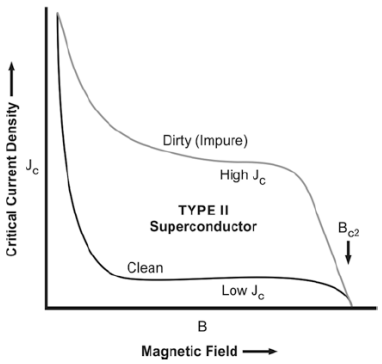

Figure 2.5: The effect of impurities on critical current versus magnetic field [2].

drops much faster for a clean superconductor as the magnetic field is increased.

2.1.4 MgB_2 Superconductor

The superconductor used in this project is a binary compound of magnesium and boride with the chemical formula MgB_2. The material's superconductive abilities was discovered in 2001 by a Japanese researcher group. The big advantage of this superconductive material is the high critical temperature compared to other conventional metallic superconductors. Figure 2.6 shows the transition from normal to superconductive state at the relatively high critical temperature of 39°K. This makes it possible to avoid the use of liquid helium, by replacing it with a close cycle refrigerator for cooling. Another big advantage is that MgB_2 is also relatively cheap compared to other HTS, due to the low price on magnesium and boron. Other HTS usually contain fractions of silver which are more expensive, and gives the MgB_2 an important competitive advantage.

There are two methods to form MgB_2 as a functional wire or tape, to make it applicable for magnet coils or other applications. The first method is a coating technique where a moving ribbon of hastelloy is coated with MgB_2. This technique provides tapes with high standard, but are not ideal for production of long length tapes. The powder in tube (PIT) technique, on the other hand, is more ideal to produce long lengths of MgB_2 wires. In this technique well prepared fine powder is packed at a high density in a metal tube, and rolled to fine sizes of wires in a series of steps of rolling and intermediate annealing to maintain ductility [2].

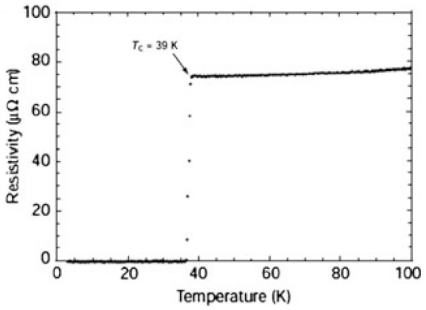

Figure 2.6: Electrical resistivity versus temperature of MgB_2 [2].

The MgB_2 are then cladded with a suited metal for sufficient mechanical support. Suitable cladding materials do not react with MgB_2, and nickel, iron and stainless steel are some of the material that are used. Copper is also incorporated on the wire to provide thermal stability and electrical protection from sudden loss of superconductivity.

2.1.5 The MgB_2 Superconductor From Columbus Superconductors

The superconductor in this project is delivered from Columbus Superconductors, where the cross section of the wire is shown in Figure 2.7. The superconductor is a multifilamentary wire with 19 MgB_2 filaments, and nickel used as the sheath material. A layer of copper is added on top of the nickel to provide thermal stability. The dimension of the cross section is 3 mm $\times$ 0.7 mm, where the height of copper and nickel is 0.2 mm and 0.5 mm respectively. The 19 MgB_2 filaments constitute an area of about 0.34 mm^2 of the cross section.

The filaments are fragile and must not be bended more than the lower bending radius or exposed to high tensile stress. A bending radius of 150mm is minimum when the copper is facing outwards, while 350 mm is the critical radius when it is bent the other way when nickel is facing outwards. A higher tensile strain of 115MPa would also damage the superconducting filaments and decrease the critical current. It is therefore important to treat the wire carefully while assembling the field winding. Rough treatment could potentially damage the filaments and decrease the critical current of the wire and make it unusable for testing.

Figure 2.8 shows the plot of the critical current density of the MgB_2 wire under different temperatures and magnetic fields. The performance of the wire is best

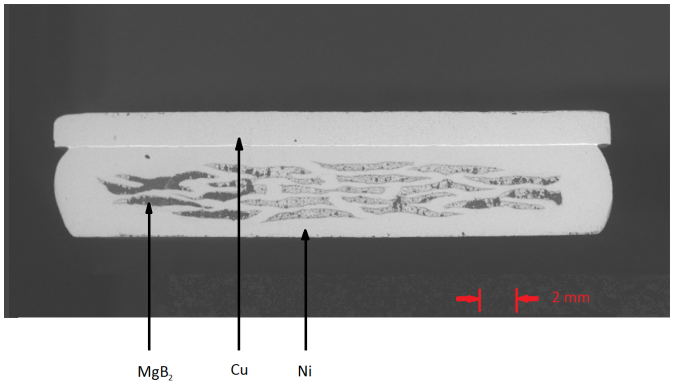

Figure 2.7: Cross section of MgB_2 superconductor from Columbus Superconductors [4].

under colder condition below 20°K such that it would be preferable to have the lowest temperature possible while testing.

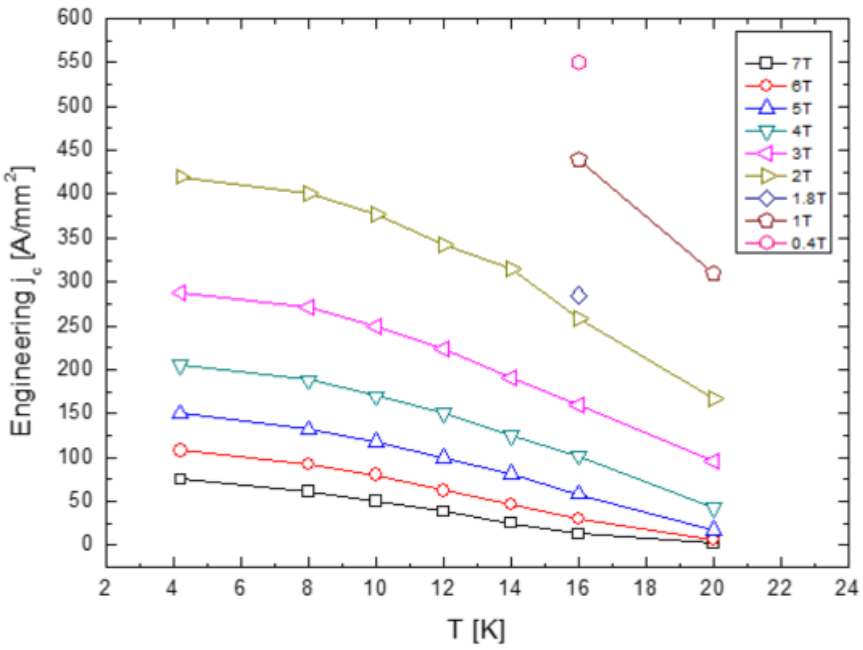

Figure 2.8: The Jc-T-B plot for MgB_2 superconductor from Columbus Superconductors [4].

2.1.6 The BSCCO Superconductor From Sumitomo Electric

A BSCCO superconductor from Sumitomo Electric is used to lead the current in the high temperature stage of the cryostat vessel. The temperature in this stage will be around 60-70°K, such that the MgB_2 will not be in the superconducting state. The superconductor from Sumitoto is made of bismuth, strontium, calcium, copper and oxygen with composition ratio of 2:2:2:3. This superconductor is also know as the Bi-2223 superconductor and have a critical temperature of 110°K. The BSCCO superconductor is therefore know to be a high temperature superconductor. The BSCCO superconductor is also available in other composition ratios with higher and lower critical temperature, dependent on the ratio. The BSCCO from Sumitomo is reinforced by a metallic lamination on each side. The wire used in this project is reinforced with a copper alloy, and the cross section is illustrated in Figure 2.9.

Figure 2.9: Illustration of cross section of the BSSCCO superconductor from Sumitomo Electric [5].

The dimension of the cross section is 4.5 mm × 0.34 mm, where the height of each copper alloy is about 50 µm. Figure 2.10 shows the critical current with respect to the magnetic field and operating temperature. For operating temperatures around 60-70 °K will the superconductor perform pretty good unless it is exposed to a very strong magnetic field. Currents of the magnitude of 100 A can be lead without any losses at this temperature.

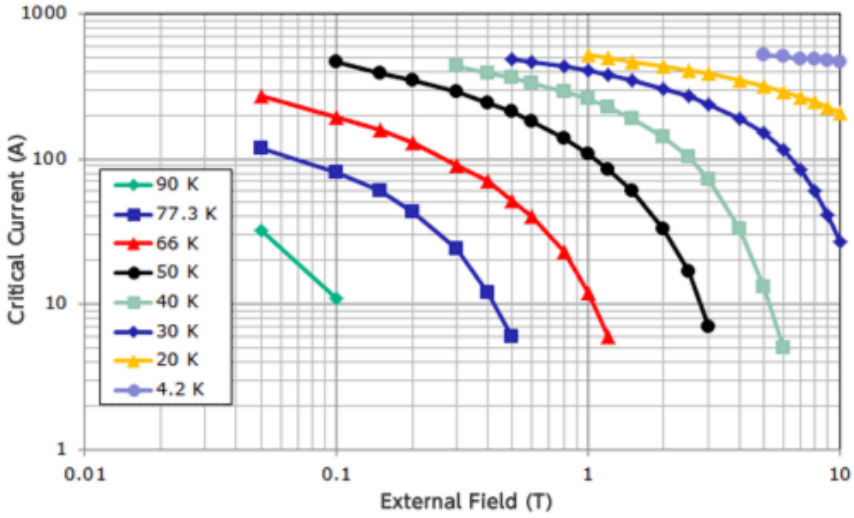

Figure 2.10: The Normalized Ic-B-T plot for the BSCCO superconductor from Sumitomo Electric [5].

2.2 Soldering

Soldering is a technique where you join two or more metal items together with a melted and flowing filler metal known as solder into the space between. This is possible because of the different melting point of the solder and the adjoining metals. The idea is that the solder has a lower melting point than the adjoining metals, such that only the solder is melted when it is heated up. When the solder is cooled down and solidified, the metal items are then "glued" together by the solder.

2.2.1 Solders

Soldering filler material also known as solder is different metal alloys with low melting points. Traditionally solders was composed of mostly lead and tin, but research has shown that lead is harmful to humans when exposed to large amounts. This discovery restricted the use of leaded solder in electrical equipment and the use of lead-free solder is now the norm in manufacturing of electronics. Lead-free solder is composed mostly of tin and other trace metals such as silver and copper. The solder used in this project is called Almit SR-37 LFM-48S and consist of 96,5% tin, 3% silver, 0.5% copper and some trace elements for reinforcement. The

melting point of this solder is 217°C, and it is completely flowing at 220°C.

Figure 2.11: Almit SR-37 LFM-48S

Figure 2.12: The cross section of a solder with flux core

To facilitate the soldering process, flux is added to the solders. This is usually done by adding flux inside the core of the wire as seen in Figure 2.12. The flux is necessary to reduce the oxides that tend to form when you have hot metals in contact with air. These oxides usually interfere with the metal-forming process of soldering and are therefore desirable to eliminate from the surface. This is done by adding flux because it react with the oxides, leaving a nice and clean metal that can form a perfect alloy with the solder. The three types of flux that are available for soldering is water-soluble, mild (No-Clean) and traditional rosin flux. The water-soluble fluxes are a recent improvement in flux as cleaning becomes much easier. A solvent is needed to remove a rosin flux, and these are usually toxic. Due to this, are water-soluble fluxes more environmentally friendly and easier to clean. The Solder that is used in this project has a core with a high performance resin flux called SR-37.

2.2.2 Electrical abilities

The electrical ability of a joint is dependent on the connection between the metals and the solder, and the dimensions of the solder between the adjoining metals. The formula for resistance is

$$R = \rho \frac{l}{A} \tag{2.4}$$

where l is the length of material, A is the area, and ρ is the materials electrical resistivity. A joint could have a bad connection because of other materials such as air and oxides are placed between the solder and the metals. These materials may have a high resistivity, and work like a insulator rather than a conductor.

Air and oxides will make the resistance of the joint higher such that more loss will be dissipated when a current is flowing through the joint. The thickness of the layer of solder do also affect the resistance. The thickness is proportional to the resistance as seen in Equation 2.4, which implies that a minimum thickness is desirable to achieve a low resistance. The resistance is also inverse proportional to the are of the joint. This makes it desirable to have a large area as possible but it is usually restricted. When joining superconductors with zero resistance are all of these factors relevant to minimize the heat dissipated in the joint.

2.2.3 Soldering irons

Soldering irons are used to heat up the adjoining metals to melt the solder and let it flow in between the two workpieces. The iron is composed of a insulated handle and a heated metal tip, where the heat is achieved electrically through a resistive heating element. Most soldering irons today are able to control the temperature by determine the thermal equilibrium. The simplest temperature control is a variable power control which changes the equilibrium temperature of the iron without measuring the temperature. Another type of system uses a thermostat to adjust the power delivered to the heating element to maintain a desired temperature. A temperature-controlled soldering iron was used for pre-soldering and a custom made iron was used to join the superconductors together in this project.

2.2.4 Solderability

Solderability of a material is defined as the ability to be wetted by molten solder. Here wetting is the formation of a relatively uniform, unbroken and adherent film of solder to the base material. The "dip and look" method and wetting balance analysis are the two testing methods commonly used to determine the solderability. The wetting balance measure and records the wetting force as a function of time and is a quantitative test. While the "dip and look" is a qualitative test performed by subjecting the components first to a steam conditioning. Then are the components dipped into the solder in a controlled fashion using a specific activated rosin flux. At the end are the components inspected and measured against specified criteria.

Nickel and copper have different solderability due to the properties of the material. Copper has a good solderability, but due to the high thermal conductivity is a high heat input during soldering required. This may result in quickly oxidization, so

proper flux is needed. Nickel has a fair solderability with a reaction rate between solder that is about two orders of magnitude slower than copper [10]. This makes it harder to adhere solder on nickel.

2.3 Electromagnetic

Magnetic fields are produced by moving electrical charges in space would for example be an electric current or currents associated with electrons in atomic orbits. The expression for the magnetic field produced by a current in an infinitely long straight wire is expressed in Equation 2.5.

$$B = \frac{\mu_0 I}{2\pi r}, \tag{2.5}$$

where μ_0 is the permeability of free space, I is the current in the wire and r is the radial distance from the wire to the location of the magnetic field. This is how the magnetic field will be produced by the field winding, by adding a lot of turns to increase magnetic field. When currents are flowing through a magnetic field, forces starts to act on these moving charges. This force is known as the Lorentz force and is expressed in Equation 2.6.

$$\vec{F} = q\vec{v} \times \vec{B}, \tag{2.6}$$

where q is the charge, v is the velocity and B is the magnetic field. When a wire carrying an electric current is placed in a magnetic field, each of the moving charges experiences the Lorentz force and together create a force on the wire. By combining the Lorentz force with the definition of electric current we end up with a force on a straight wire that are expressed in Equation 2.7.

$$\vec{F} = I\vec{l} \times \vec{B}, \tag{2.7}$$

where l represent the length and direction of the wire, I is the current and B is the magnetic field. Since the force is a cross product of the direction of the current and the magnetic field, the direction of the magnetic force can be found by using the right hand rule as illustrated in Figure 2.13.

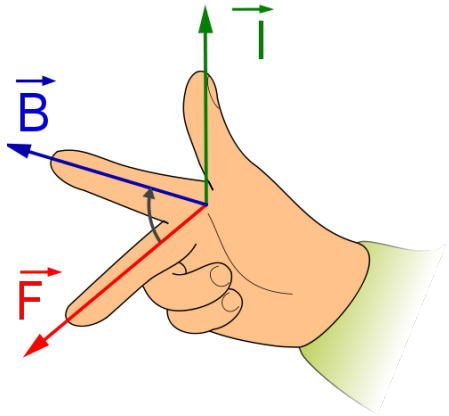

Figure 2.13: The right hand rule.

The field winding in this project will experience large magnetic forces trying to deform it to a ring. These magnetic forces needs to be considered when designing the test setups for the field winding.

2.3.1 Inductance

Another electromagnetic property of the field winding is the inductance. Inductance is the behavior of a coil resisting any change of electric current through the coil. The relationship between the inductance, electric current and voltage is given in Equation 2.8 and is derived from Faraday's law of inductance.

$$V = L\frac{di}{dt} \tag{2.8}$$

Inductance is measured in henrys where the unit is named after the American scientist Joseph Henry. The energy stored in an inductor is given by Equation 2.9.

$$W = \frac{1}{2}LI^2 \tag{2.9}$$

Chapter 3

Assembly of Rotor Field Winding

Introduction

The ten individual coils wounded as a double pancake need to be assembled together both electrical and mechanical. This chapter describes the procedures that were done to complete the field winding, and the challenges that occurred during the assembly.

Each individual coil has 208 turns wounded as a double pancake [7]. The total number of turns of the field winding would then be 2080, as the coils will be connected in series. The assembly was done in steps where one coil was first glued with epoxy and then joined electrically with the previous coil by soldering. This procedure was repeated until all of the ten coils were connected. The epoxy used was Stycast 2850 FT mixed with the hardener Catalyst 24 LV (weight ratio 1:0.07), and was chosen for its good thermal conductivity. This is the same epoxy used for turn-to-turn insulation, and was also used in a previous project completed in 2009 [11]. A good thermal conductivity of the epoxy is crucial to cool down and maintain a low temperature below the critical temperature of the superconductor. This reduces the risk of quenches as the heat would be faster transported away from the coil to the cold head.

The solder used was Almit SR-37 LFM-48S and it consists of 96,5% tin, 3% silver, 0.5% copper and some trace elements for reinforcement. The melting point of this solder is 217°C, and it is completely flowing at 220°C. This was chosen as a compromise of not using a lead-based solder, low melting temperature and the ability to stick to nickel [12]. The soldering procedure was developed as a part of a specialization project in the fall of 2015 [12], and was used to join the individual

coils together electrically. This procedure insured that the layer of solder between the superconductors was minimized, making the resistance as low as possible.

3.1 Joining the Coils by Gluing and Soldering

The first coil was glued on a thermal interface made of copper. The thermal interface will be connected to the cold head, and cool down the field winding more effectively. The interface is also the mechanical structure that keeps the field winding together during assembly. It is made up by a copper plate with the shape of the coils, with an additional space on top to connect the cold head. Copper teeth are mounted on the inner edge to fit each individual coil. The teeth will make the coils line up perfectly on top of each other and increase the cooling surface to the field winding. The bottom of the thermal interface is shown in figure 3.1.

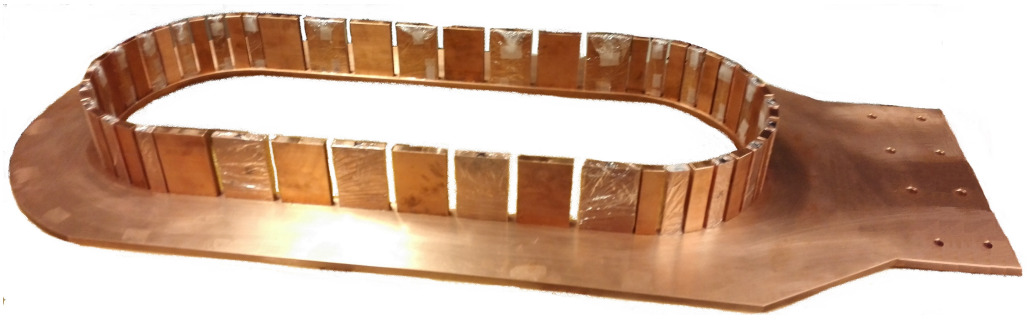

Figure 3.1: The bottom of the thermal interface with all the copper teeth mounted on the inner edge.

An identical copper plate was placed on top of the field winding to increase the thermal conductivity. Every other copper teeth seen in Figure 3.1 was mounted on this plate, to distribute the cooling better and more even. The teeth are lower than the field winding to prevent an electrical connection between the two plates. This was done to prevent induced current between the plates when the field winding is tested.

During the assembly of each coil, was every teeth mounted on the copper plate at the bottom as seen in Figure 3.1. This was necessary to insure that less epoxy would drain, but also leave a perfect groove for the teeth when they was mounted on the top plate. Every other copper tooth was therefore covered with a regular cling film to prevent them from attaching the epoxy. The other half was covered with kapton tape for electrical insulation between the field winding and the copper teeth. This tape was chosen because it is very thin and would maintain a good

thermal conductivity between the interface and the superconducting field winding. There was not placed any kapton tape between the teeth and the first coil.

Pieces of fiberglass was places between the interface and the first coil to prevent an electrical connection. The pieces was about 4 mm thick and was placed similar around the thermal interface as seen in Figure 3.2. The fiberglass pieces were also placed between the coils to prevent shorting any turns from the one coil to the other.

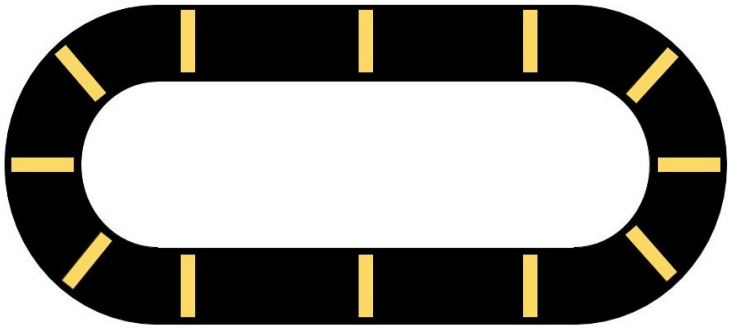

Figure 3.2: Placement of the fiberglass pieces between the indivdual coils.

Epoxy was applied to the thermal interface and at the bottom of the first coil. Before the epoxy was added to the bottom of the first coil, cavities between the wires from the winding procedure was refilled. A small portion of epoxy was heated in a water bath to make the viscosity lower such that the epoxy would drain more easily. This made the epoxy able to drain into the cavities and fill them. After both surfaces were covered with a layer of epoxy, the coil was flipped and placed on top of the thermal interface. The coil was pushed down by adding weight on top of it. This was done to minimize the layer of epoxy and to make sure that there were no gaps between the coil and the thermal interface. A piece of teflon, shaped similar to the coil, was placed on top to protect the superconductor wires. Masses of 10 kg was then placed around the surface to make an even pressure over the coil as seen in Figure 3.3.

The epoxy had a cure time of 16-24 hours in the room temperature of 25°C. The weights stayed on the coil during the night and were removed the next day when the epoxy had cured. The next coil was added on top of the first coil by doing the same procedure as described above.

One problem that occurred was that all the individual coils were leaving a gap between the copper teeth along the straight edge. In other words was the inner

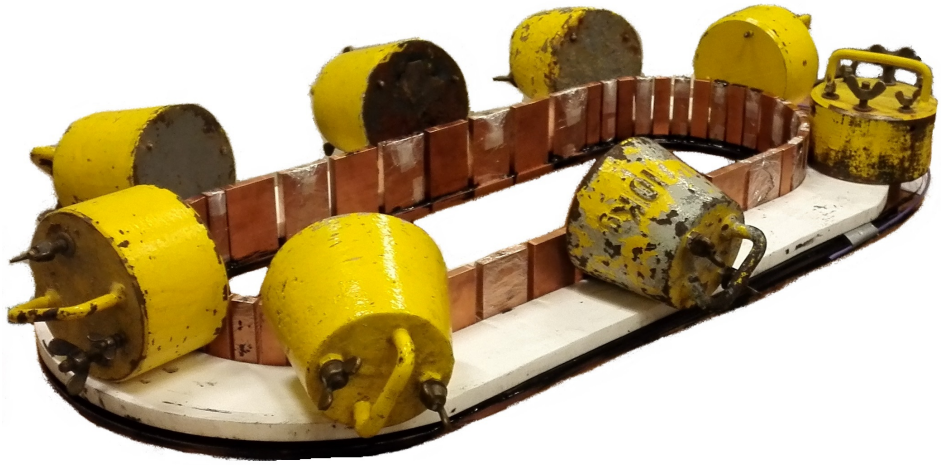

Figure 3.3: The first coil glued to the thermal interface with Stycast 2850 FT. The layer of epoxy was minimized by adding weight on top of the coil to push it down.

edge of the coils not perfectly shaped to the straight alignment of the copper teeth on the thermal interface. This happened because of difficulties to keep the wires straight during the winding procedure. The gaps were filled up with pieces of superconductor and extra epoxy, as shown in Figure 3.4. In this way the same material properties were present here as the rest of the field winding. The main reasons to fill these gaps were to make sure that the copper teeth were connected to the field winding for better cooling.

Figure 3.4: The pieces of superconductor that were placed between the tenth coil and the copper teeth.

3.1.1 Soldering

As soon as the second coil was glued and the epoxy was hardened could the first joint be made by soldering. A good soldering technique to join the coils were required to achieve a low resistance as possible between the coils. This minimizes the heat dissipated in the joints and reduces the risk of exceeding the critical temperature. The consequences of a poor joint might lead to quenches of the superconductor and possibly destroy the coil if it is not detected fast enough. The soldering procedure was done in two stages: a pre-solder stage and a joining stage.

3.1.2 Pre-soldering

The soldering process starts with some preparation of each wire. Sandpaper of size P800 is used to make the surface rough and remove oxides from the metal such that the solder will adhere easier. Isopropanol is used to remove the sanding dust and clean the surface. After this is done the wire is pre-soldered with the solder Almit SR-37 LFM-48S with the correct temperature. The superconductors are joined by a overlapping joint where copper ia connected to nickel as illustrated in Figure 3.5. This implies that one end of the coil is pre-soldered on nickel, and the other on copper. The joint are made this way because it is the most space efficient way and also the easiest method as long as the solder adheres to nickel. Removing the copper from the nickel and solder nickel to nickel was discussed but was found to be too risky. This procedure would increase the risk of damage the superconductor while removing the the copper from the nickel, and was therefore not implemented. The pre-soldering was done by a regular temperature controlled soldering iron, where the temperature was regulated to about 275°C.

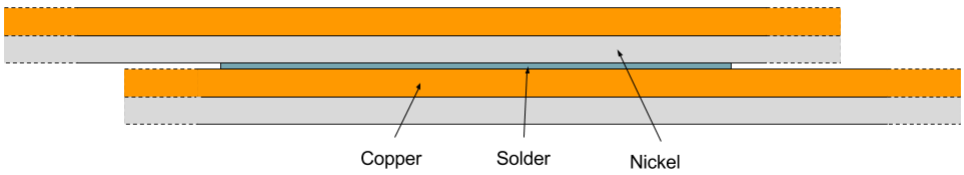

Figure 3.5: Illustration of a MgB_2 joint

Solder was added on the wires such that the length of the joint would be the same as the custom soldering tool. About 120 mm of the wire was covered with solder, and it was important to not adhere solder any longer than this. Solder outside of the soldering tool might not melt, and make it impossible to reduce the thickness

of the solder. This would increase the resistance in the joint and produced more undesirable heat when current flow through.

The superconductor was held by a holder made of a firesafe material during the whole pre-soldering procedure. The design of the holder is shown in Figure 3.6a. The holders were place in holes such that the distance between became the desired 120 mm as illustrated in Figure 3.6b. This made it possible to add a thin layer of solder on each end of the coils without damaging the superconductor.

(a) Custom made soldering holder for superconductors.

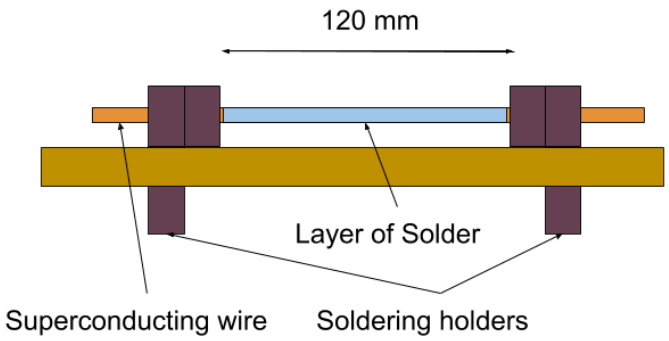

(b) Illustration of how the superconducting wire was held by the soldering holder during the pre-soldering procedure.

Figure 3.6: The soldering holder.

The solder from Almit used to pre-solder is melting at 217°C, and liquefies at 220°C. However a higher temperature of the soldering iron was needed, becasue of the high thermal conductivity of copper and nickel. An iron temperatures of 275°C was high enough to melt and attach the solder on the surface of the superconductor. The iron tip was moved slowly upwards the wire such that the solder would attach properly, but not too slowly, because more heat would increase the risk of delamination.

3.1.3 Joining the Coils with Soldering Tool

After the pre-soldering, the two superconductors at each end of the coils were placed in the soldering tool with nickel facing out. The soldering tool used in this project is a custom soldering iron designed to solder MgB_2 superconductors. An illustration of the tool is shown if Figure 3.7. The tool is made from a high power

soldering tool, where the tip is replaced with a designed copper plate. The copper plate has eight brass screws and two placement barriers connected to work as desired. A second copper plate is attached with springs and wingnuts on the brass screws to apply pressure on the superconductors while soldering. The pressure is essential to make the joint as good as possible by reducing the thickness of solder. The heat is only applied from the copper plate beneath the superconductors, and is controlled manually by unplugging the iron. No thermometer is installed on the iron, so temperature measurements was done separately.

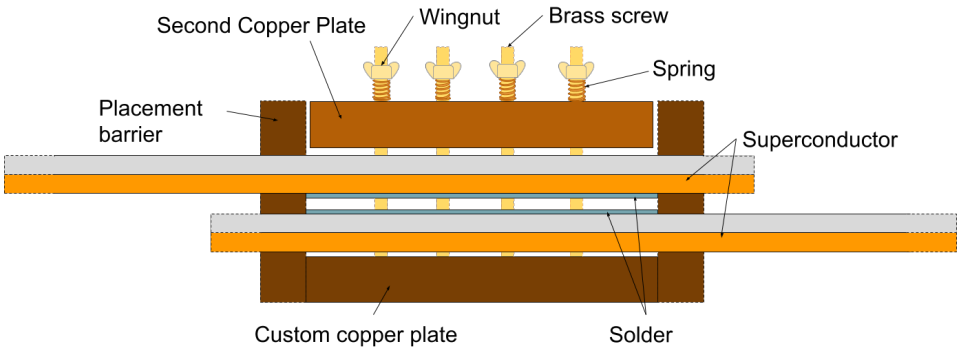

Figure 3.7: Illustration of the cross-section of the soldering tool.

The superconducting wires were overlapping each other and held in place by the placement barriers at each end of the soldering tool. Temperature was measured by three thermocouples type K connected to an Agilent 34970A data logger. The positions of the thermocouples were is shown in Figure 3.8 and heat profiles of the soldering processes can be found in Appendix A. A maximum temperature of 250-260°C was used to ensure that the solder got liquefied such that the springs could compress the layer of solder to a minimum. A piece of aluminum foil was also placed between the soldering tool and the joint to avoid the solder to attach to the soldering tool.

Optimal pressure was applied from the eight springs on top of the second copper plate. The force from every spring is proportional to the distance the spring is deformed from its equilibrium length, and is given by

$$F = -kx. \tag{3.1}$$

Here k is the spring constant, F the force and x the displacement distance. In this case the x will be the distance the springs are compressed by the wingnuts. The number of turns of the wingnuts is proportional to the force as long as the screw threads are not damaged. Each wingnut was turned 2.5 revolutions from top of

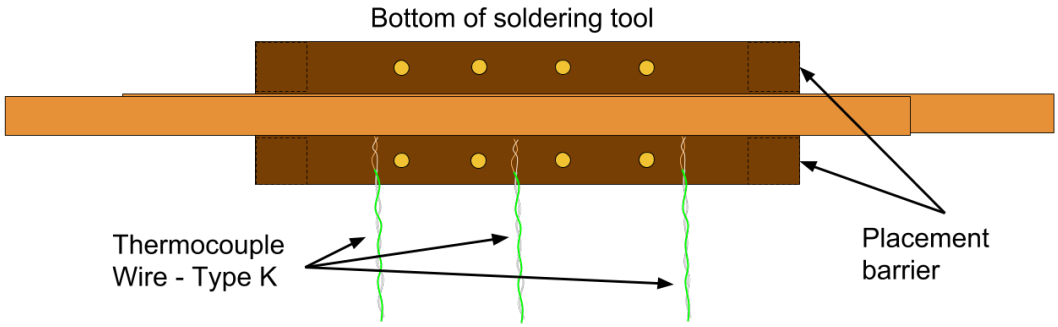

Figure 3.8: Illustration of a MgB_2 joint inside the soldering tool. The position of thermocouple-wires that are measuring temperature are also shown.

the spring to compress it. This proved to be the best pressure as the upper copper plate of the soldering tool pushed with a great force without loosing mobility. This procedure was validated in a specialization project [12] conducted during fall 2015, by measuring the thickness of the layer of solder.

One challenge that occurred was that the wires of the coils were supposed to be solder together in a fixed position. This was solved by fastening the soldering tool to a vise with a ball joint for mobility as seen in Figure 3.9. The vise was fastened to a pallet placed on top of a rolling table such that the soldering tool could move around. Pieces of wood were placed in between the table and the pallet to elevate the soldering tool to the correct height.

This procedure was repeated for the next eight coils, with gluing and soldering done for each coil. As more coils were assembled the surface got more uneven. This became a problem as there were minor gaps with air between the field winding and the next coil that was added. This was solved by using screw clamps to force them together. Before the tenth coil was glued, every other copper teeth wrapped in cling film was removed from the bottom copper plate to be mounted on the top of the thermal interface.

Figure 3.9: The first and second coil soldered together by the custom soldering tool. The soldering tool was held by a vise with a ball joint for mobility.

3.2 Assembly of the Second Thermal Interface

After the last coil was added to the field winding two problems were detected. Due to the uneven, but necessary pressure from the screw clamps, did some parts of the field winding not reach over the height of the copper teeth by some few millimeters. This also implies that the surface was uneven and a flat copper plate on top of it would not fit perfectly. The first problem was solved by using a milling machine to make grooves for the copper teeth that were higher than the field winding. Grooves with a depth of 5 mm were milled to fit the surface of the field winding. In addition were the opposing copper teeth of the grooves cut which decreased the height by 5mm. Due to the uneven surface big gaps were still a problem when the plate was placed on top. This was solved by bending the copper plate by a hydraulic press machine. It turned out to be more difficult to fit the copper plate perfectly, but after a lot of bending back and forth was a sufficient result achieved. This result made the plate fit better but there were still gaps in between. Figure 3.10 shows the location and the sizes of the gaps represented by the measurements

in the figure, when a small force was applied to the copper plate. The gaps became 1.9 and 1.4 mm when 20 kg was placed in front and 10 kg in back, as shown in Figure 3.10.

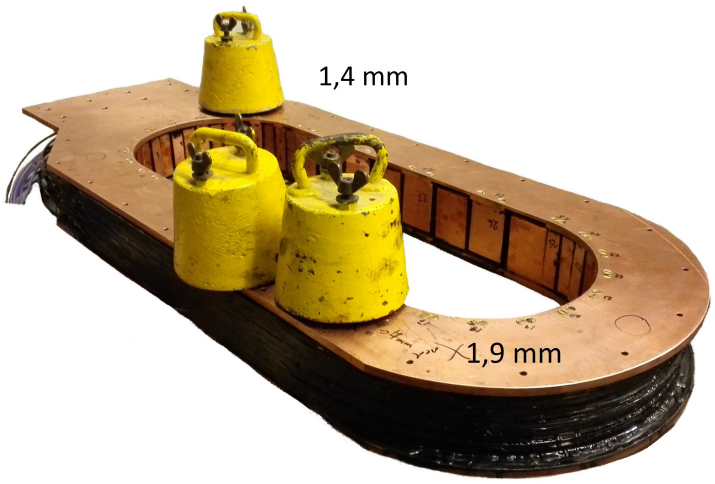

Figure 3.10: The length of the gaps between the thermal interface and the field winding when a small force is applied.

Since there was such a small force needed to push them together even further, was it decided to glue the thermal interface with two layers of fiberglass in between the 1.9mm gap. Two layers of fiberglass would reduce the gap to less than 0.9mm, as the thickness of each fiberglass piece is 0.5 mm. Epoxy between the fiberglass pieces would add up some more height and decrease the gap even more. A lot of epoxy was used to be sure the that the gap would be filled, and screw clamps with a minimum of pressure was applied. This made the copper plate bend perfectly and fit the top of the field winding. The clamps were removed the next day, when the epoxy was hardened.

3.3 Cooling the Joints

There will be heat dissipated in the joint due to the resistance in the solder, copper and nickel when current flow from the one superconducting coil to the next. Cooling of these joints is therefore extremely important to avoid quenches and a potential failure of the field winding. Two pieces of copper were designed to be mounted on the thermal interface to increase the thermal conductivity from

the joints to the cold head. The two pieces were made of the same material as the thermal interface, and the design is shown in appendix B. Groves, as shown in Figure 3.11, were made in the thermal interface by a milling machine to attach the pieces.

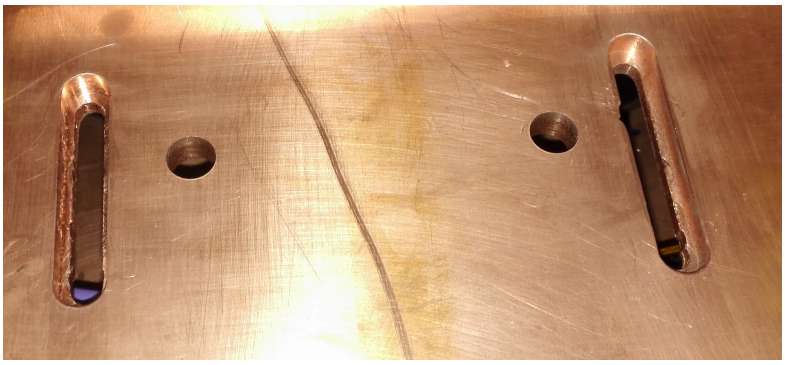

Figure 3.11: Grooves made in the thermal interface to attach the cooling pieces for the joints

One piece was placed behind the joints while the other was placed in front of the joints. The pieces was then pushed together to get a good thermal connection to the joint. The colling pieces were fastened with hexagon screws to the thermal interface, and locked in their positions as shown in Figure 3.12.

Kapton tape was used to insulate the wires such that none of the wires were shorted to the copper. The tape is very thin, such that a good thermal connection to the copper was still maintained. The copper pieces and the insulated wires were also covered with Apiezon N vacuum grease to improve the thermal connection between them. This grease was used because it is recommended as a good cryogenic vacuum grease that can withstand frequent cycling between cryogenic temperatures as low as 1°K and up to 300 °K.

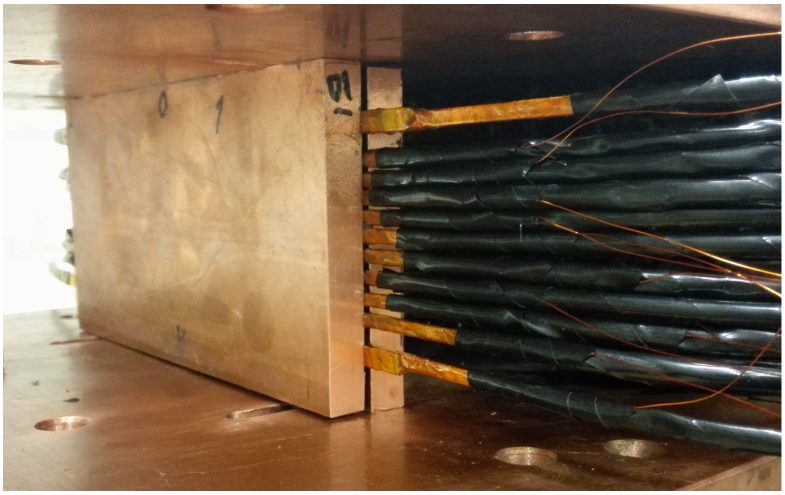

Figure 3.12: The joints connected to the thermal interface by two pieces of copper at each side.

3.4 Making Parallel Plates for Mechanical Support

Magnetic forces will act on each current carrying wire with a force of a magnitude calculated from Equation 2.7. This happens because of the charges moving in a strong magnetic field. Since the field winding is shaped like a racetrack, would these forces eventually try to bend the field winding to a circle. A mechanical support strong enough to withstand these forces is therefore required to be installed around the field winding to be sure that it is not torn apart. A flat and plain surface on each side of the field winding was made such that a mechanical support made of stainless steel could support the field winding and resist the magnetic force. It was important that these two surfaces were perfectly parallel and ninety degrees to the field winding, such that the design of the mechanical support would work optimally. Something similar to a mold was made to satisfy these criteria and the design can be found in Appendix C. Since the surfaces of the coils were uneven and slightly bending inwards from the middle, were pieces of fiberglass used to fill the gaps at each end. A illustration of this is shown in Figure 3.13. This was done to reduce the thickness of epoxy in fear of cracking if the layer became to thick. A piece of fiberglass covering the whole area was placed closest to the mold to make sure that the surface became even.

The sides of the mold were covered with cling film to ensure that it would not stick to the epoxy. A layer of mold release was also added into the grooves of the

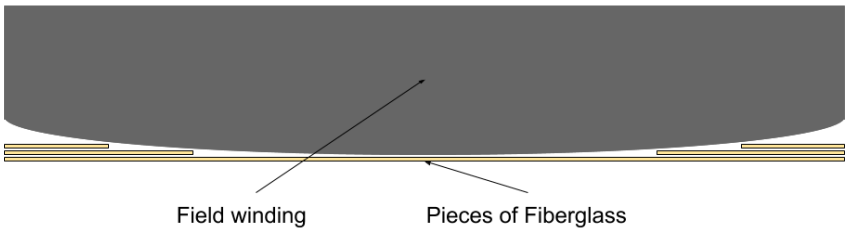

Figure 3.13: Illustration of the three layers of fiberglass added to minimize the layers of epoxy

mold for the same reason. Figure 3.14 shows how the mold was placed around the field winding. The grooves were milled 479 mm apart such that the plates were perfectly parallel when the mold was assembled. A lot of epoxy was used to cover the fiberglass plates and placed between the mold and the field winding. More epoxy was poured into the gaps to fill up the cavities and make a solid plain surface on each side of the field winding.

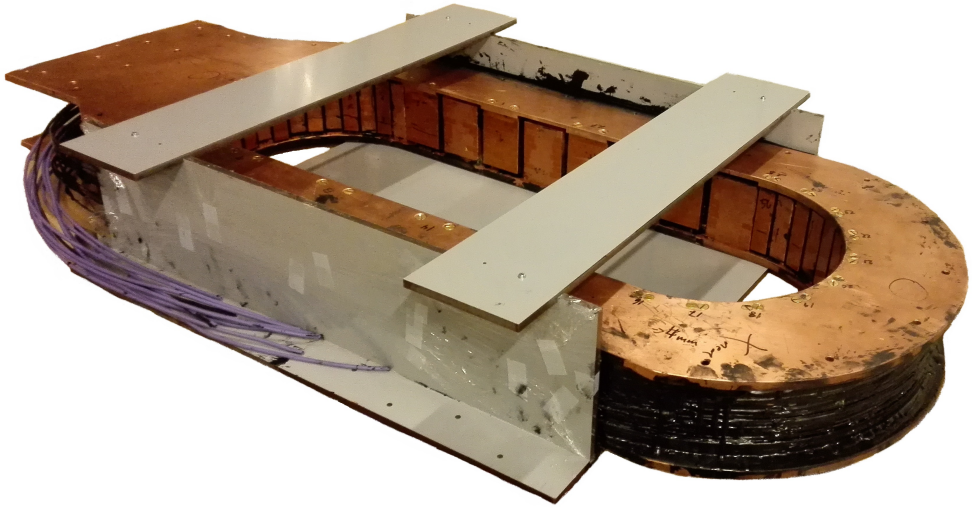

Figure 3.14: The field winding with the mold placed around.

Because the mold was not closed on each side, was epoxy spilled on each side. It was therefore necessary to refill epoxy, as some of the epoxy had flown out through the sides. The refilling was done after adding some duct tape to close each end to make sure that nothing was spilled. After the refilling were all the remaining gaps and cavities filled with epoxy, such that it would make a perfect contact area for the mechanical support. The epoxy spilled on top and bottom

of the thermal interface was also sanded away with a pneumatic air belt sander. This was necessary to make it possible to place the mechanical support around the thermal interface. The plain surface is shown in Figure 3.15

Figure 3.15: Surface after the mold was removed and epoxy spills were sanded away

3.5 Designing the Mechanical Support

When the outer surface of the field winding was completed, was the width of the field winding measured such that the mechanical support could be designed. The support is made of stainless steel and the dimensions of the pieces are found in Appendix D. It is made of stainless steel because this material is non-magnetic, such that it would not be affected by the strong magnetic field produced by the superconducting winding during tests. Figure 3.16 shows the mechanical support assembled together. The pieces were designed in AutoCAD and cut by a water jet cutter. The water jet cutter made it possible to be extremely precise, and cut the mechanical support with an accuracy of one tenth of a millimeter.

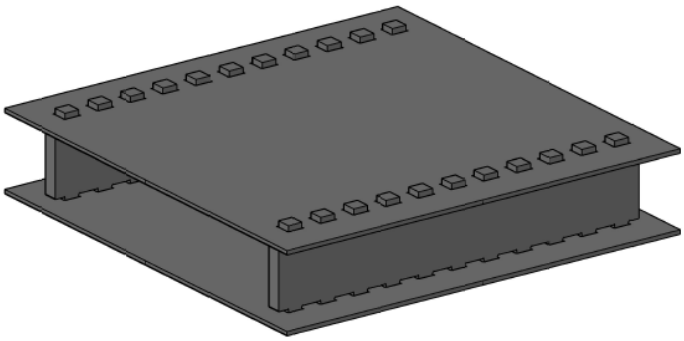

Figure 3.16: The mechanical support of the field winding designed in AutoCAD.

Based on simulation of the magnetic field produced by the field winding, was an overestimation of the force calculated based on equation 2.7. The force is calculated with a current of 200 A per turn and a magnetic field of 1.2 T, which is the average magnetic field strength over the cross-section of the field winding.

$$\vec{F} = I\vec{l} \times \vec{B} = 200 \cdot 2080At \cdot 0.5m \cdot 1.2T = 249.6kN \tag{3.2}$$

This calculation is also simplified by assuming that all magnetic field lines cuts the wires at exactly ninety degrees in the same direction. In reality will the outer wires actually be pushed inwards due to the opposite direction of the magnetic field, and therefore cancel out some of the forces outwards. This estimation is therefore an overestimation.

The mechanical support should at least withstand a force of the size calulated in Equation 3.2. Based on calculation of the mechanical properties of the material, should each plate withstand 682 kN. This is calculated from the 0.2% offset yield strength of the material. The tensile strength is also assumed homogeneous between the holes in the plates. The material used is ductile in cryogenic temperatures, such that a brittle fracture is not likely [13].

3.6 Soldering BSCCO High Temperature Superconductor

A high temperature superconductor was soldered at both ends of the field winding. The cryostat will have two temperature stages where the inner stage will reach a temperature down to about 20°K, and the outer stage will have a temperature about 60-70°K. A HTS is therefore needed to lead the current from the warmer outer stage to the colder inner stage where the field winding will be. It would be possible to use copper as well for this task, but this would imply a relative big cross section of the copper wires. This is not wanted as a big cross section would also imply more heat transferred from the ambient temperature.

A BSCCO HTS from Sumitomo was used to solve this problem as the superconductor material has a critical temperature at 110°K. Three wires in parallel were soldered on each end to be sure that the current in each wire would not exceed the critical current at the operating temperature and magnetic field. Three wires were used based on the critical current found in the plot in Figure 2.10. An estimated temperature around 66°K based on measurements from an earlier project [11], and a magnetic field of 0.25 T were used to find the critical current. The magnitude of the magnetic field is based on simulations in COMSOL multiphysics. These numbers represent a worst case scenario, where the hottest spot would be were the highest magnetic field is present. In reality the coldest spot of the HTS is where the highest magnetic field is present and vice versa. Based on the worst case scenario, would the BSCCO wire have a critical current of approximately 100A. To be able to lead 200 A with some safety margin were three wires chosen. Not only for safety reason but also to have the opportunity to test the field winding with even higher current were three wires chosen. The drawback by having more wires is that it implies a bigger cross-section with higher heat transfer capability.

Because the BSCCO superconductor wires are wider were some modifications of the solder tool made. The width of the BSCCO wire is 4.5 mm which is 1.5 mm wider than the MgB_2 wire. Two new placement barriers were designed and made

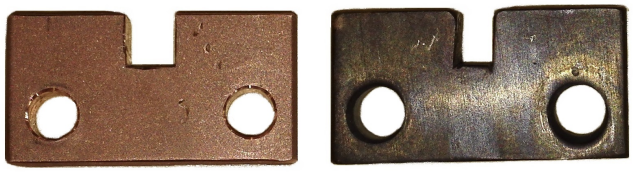

Figure 3.17: The new placement barrier for the BSCCO superconductors is to the left, while the old for MgB_2 is to the right

to make it possible to use the soldering tool. The new placement barriers are shown to the left in Figure 3.17 next to the old one. The spacing of the placement barrier was chosen to be 5mm, such that the BSCCO wire would fit.

A soldering test was conducted to see if it was possible to solder three BSCCO wire together with a MgB_2 wire. The procedure was almost the same as described in Chapter 3.1.1, with a pre-soldering stage before the wires were joined with the soldering tool. Here one of the three BSCCO wires and the Mg_2 wire were also pre-soldered on both sides because it would be joined from both sides. Two BSCCO wires were soldered to the copper of the MgB_2, while the last was soldered to the nickel. The soldering test was successfully completed and the modified soldering tool worked exactly as it should.

Figure 3.18 shows the first soldering of the end of the field winding. Two wires were soldered on the outer side, while the last one was solder on the inner side. The soldering tool was still held by a vise connected to a rolling table to place it in a perfect position. All wires were pre-soldered and joined by the soldering tool with a maximum temperature of 250°C. The second end was also soldered similarly as described above.

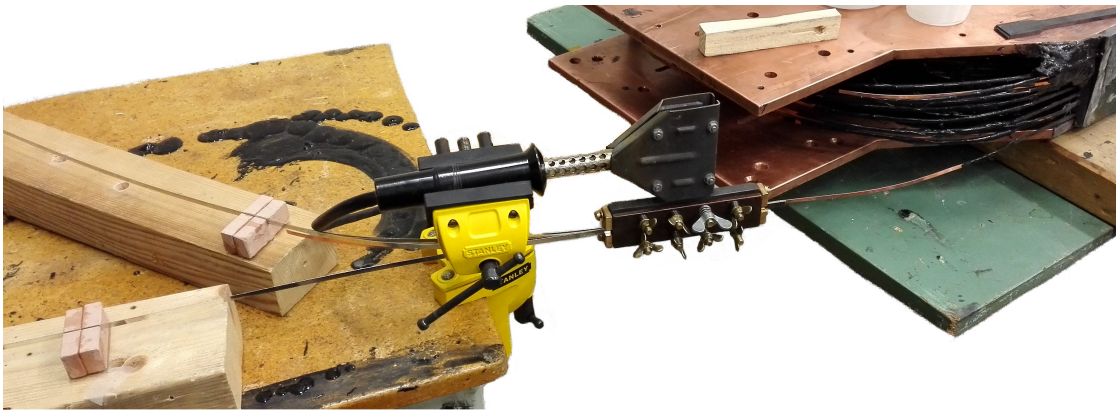

Figure 3.18: Soldering of BSCCO HTS wire at the end of the field winding

3.7 Copper Termination

The termination of the field winding will be connected to a copper bus bar connected to the current source. The termination will be fastened by a screw and nut to the copper bus bar. A design to make it possible to fastened the three HTS to this bus bar was therefore needed. A piece of copper soldered to the BSCCO superconductor was the solution for this. The copper termination soldered to the BSCCO HTS is shown in Figure 3.19.

Figure 3.19: The design of the copper termination. The termination is soldered to three BSCCO HTSs.

The soldering tool was also modified to do this task. Figure 3.20 shows how the termination was placed inside the soldering tool with two custom made placement barriers and a shorter plate on top pushing it all together. The length of the joint was here decided by the length of the copper piece. Since there will be losses in copper regardless of the thickness of the layer of solder, was a long joint therefore not as critical as before. The length of the copper termination was therefore decided by a practical reason. It was chosen to be long enough to hold it during assembly of the cryostat. The terminations are going to be led through a hole and up to the copper bus bar. To make it practical the length was decided to be longer than this hole such that it is possible to hold the termination from one side while connecting it to the bus bar on the other side. This resulted in a copper termination with the length of 70 mm. The dimensions of the copper termination can be found in appendix E.

The thickness of the termination was decided to be 5.5 mm to be sure that it was wider than the wires. It was on this surface the wires were soldered on the copper. The wires were divided as before with two wires soldered to one side and the last one to the other side.

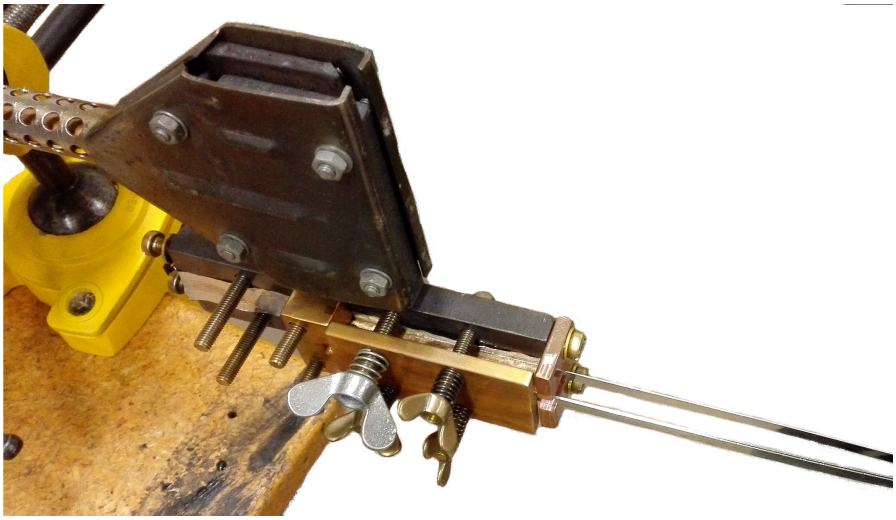

Figure 3.20: Soldering the copper termination to the HTS wires.

3.8 System for Voltage Measurement

A system to measure voltage was implemented to the field winding to be able to calculate the resistance in every joint, and to control that every individual coil is working as it should. A measurement point for voltage was added on each side of every joint that the current would flow through. Enameled copper wires with a diameter of 0.23 mm were soldered at the measurements points with the Almit solder, the same solder used for joining the superconducting wires. Measurements points were added at each side of the termination and the joint, between the BSCCO and MgB_2 superconductor due to the arrangement of the HTS wires. This makes it possible to measure the voltage over both joints where the HTS wires are connected in parallel.

The wires were connected to three terminal strips mounted to the thermal interface, as seen in Figure 3.21. A thin layer of Stycast epoxy was used to glue the terminal strips to the thermal interface to ensure that it was attached and cooled with the rest of the field winding. The termination strips were mounted because they made it possible to use the wires that were already mounted in the cryostat. These wires are connected to two 25 pin D-sub female connectors outside of the cryostat, which make it really simple to connect a data logger to collect data from the measurements.

The voltage measurement system outside the cryostat consists of two shielded 25 pin D-sub male cables connected to two 20-Channel plug-in modules and are shown in Figure 3.22. The two plug-in modules are connected to an Agilent 34970A data

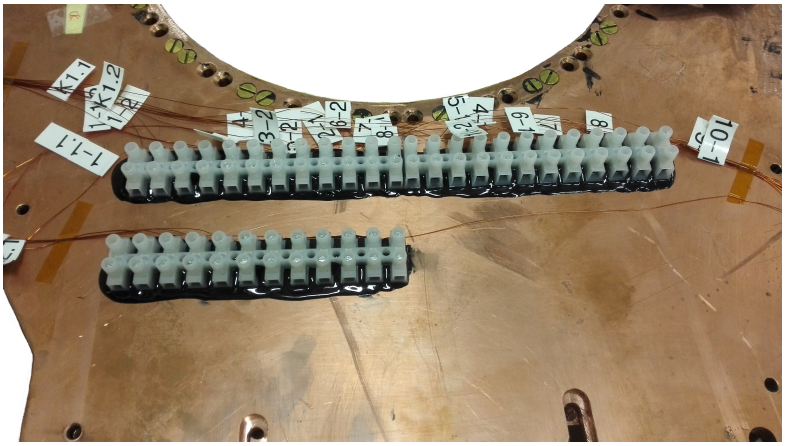

Figure 3.21: The three terminal strips glued to the thermal interface with all the enameled copper wires connected

logger to collect and store the measurement to a computer. Two of the wires from the second D-sub were the current wires of the Cernox sensors and connected to a current source. The current was measured by a current channel in the second plug-in modules. Appendix F shows how all the wires are connected to measure the voltages over each joint and coil. 34 of the 50 available in the cryostat were used to measure voltage. The thermal conductivity for these wires are calculated in Appendix G and turned out to be about 1W. This calculation is a simplification that assumes a linear temperature gradient over the length of the wire. This would most likely not be the case in reality, but the calculation gives a clue about how much heat that is going to be transfered by the wires. The wires were therefore thermally anchored by attaching the wires to the copper shell, to reduce the heat transfered to the field winding. Some of the heat would then be transfered to the copper shell that is connected to the second stage of the cool head.

Figure 3.22: The two 25 pin D-sub cable connected to two plug-in modules for an Agilent data logger.

3.9 The Suspension of the Field Winding

A suspension to make the field winding fit into the cryostat was designed. Four epoxy plates, shown in Figure 3.23a, were already made to hold the the field winding. The two pieces in the middle, shown in Figure 3.23b, fit perfectly inside the thermal interface, such that the field winding will be supported by these while hanging.

Four rods of stainless steel with a diameter of 16 mm were made to fit the suspension already mounted in the cryostat and the holes made in the epoxy plates. It was desirable to have these rods as big as possible to withstand the weight of the field winding with a highest safety factor as possible. Spacers where also made to make sure everything stayed in the right position. These spacers were made by cutting pieces of a stainless steel pipe and were placed outside the rods. The length of the spacers was critical to get right, such that the field winding would be positioned underneath the cold head in the cryostat. An illustration of the design of the suspension is shown in Figure 3.24.

Grooves in the mechanical support were also milled to fit the suspension. The grooves were made oblong in the horizontal direction for flexibility during assembly. This made it possible to move the mechanical support sideways with respect to the rods when the mechanical support was attached around the field winding. The height of the grooves were made 16 mm such that the mechanical support would hang perfectly on the rods. Holes for cotter pins were made in the rods placed in the cryostat suspension, while screw thread were made on the rods at the bottom

(a) The suspension assembled together to check that the length of the spacers are correct.

(b) The two middle pieces of the suspension supporting the field winding

Figure 3.23: The suspension for the field winding .

to make sure everything were held together. Screw threads were chosen for the bottom rods to be able to fasten the suspension as tight as possible to the field winding.

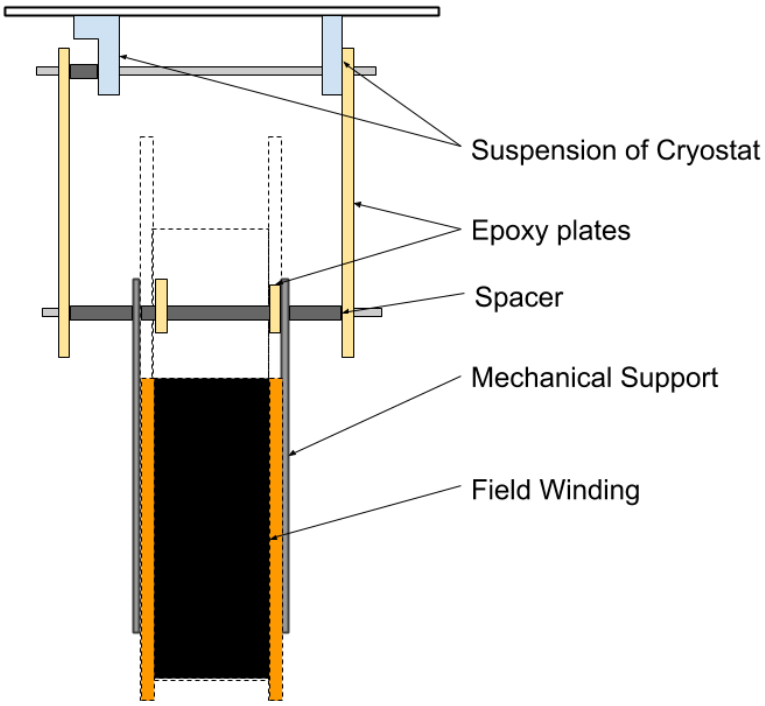

Figure 3.24: Illustration of the design of the suspension that keeps the field winding in the correct position

3.10 System for Temperature Measurement

Two Cernox 1070-SD-HT-4L sensors were installed to measure the temperature of the field winding. The Cernox sensor is a cryogenic temperature sensor made by Lake Shore Cryotronics with a temperature range from 100°mK to 420°K. The sensor is a thin film resistance with high sensitivity at low temperatures. The typical sensor accuracy is ±9°mK at 20°K, such that the temperature can be measured with a very high accuracy. Each sensor are calibrated individually and delivered with calibration data shown in Figure 3.25. The two sensors used in this project are calibrated for temperatures from 330°K and down to 3.6°K.

One sensor was placed at the bottom of the field winding (X106350) while the other was placed on top near the attachment of the cold head (X106341). This should give a representative temperature measurement for the whole field winding, as these two point would most likely be the warmest and coldest point of the field winding during cool down. No more than two Cernox sensors were installed due

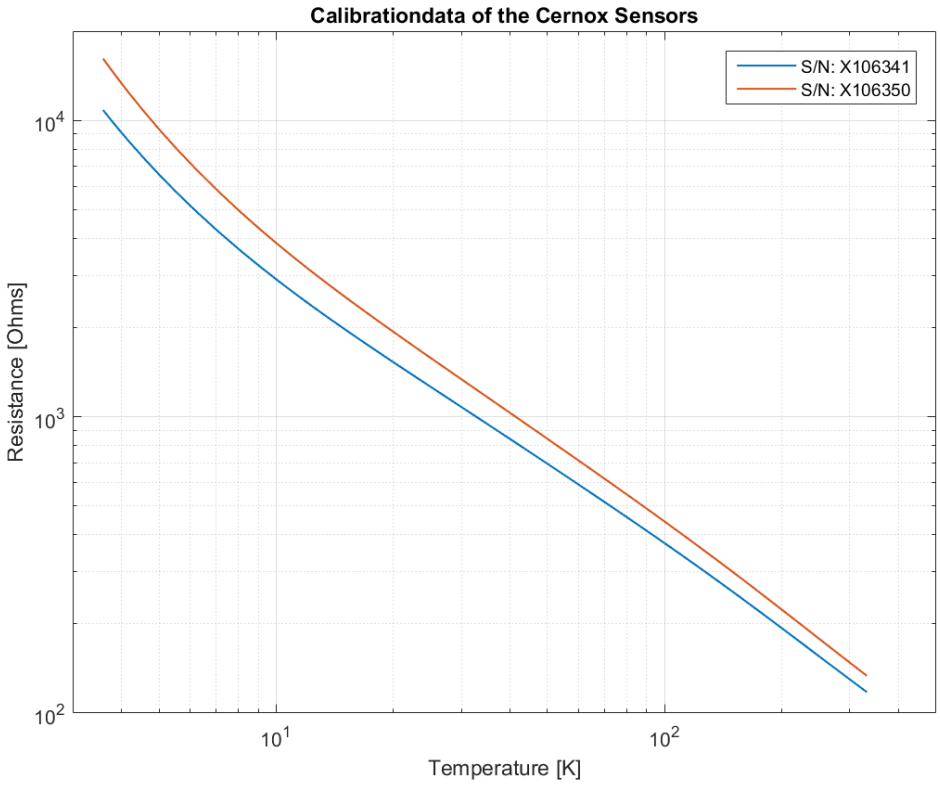

Figure 3.25: The calibration data of the two Cernox temperature sensors. The resistance is plotted vs. the temperature.

to the high cost of the sensors. Cheaper thermocouples could have been used, but experiences from an earlier project [11] concluded that it was difficult to get reliable measurements. Errors of over 10°K was discovered which is not acceptable. It was therefore decided to only use Cernox sensors to get accurate temperature measurements.

A proper mounting of the sensors are critical for optimum performance. The mounting areas were cleaned with an isopropanol rinse before mounting. The bottom sensor was installed by a custom made mechanical holder placed on the bottom of the field winding. The holder are shown in Figure 3.26 and are made of fiberglass to avoid electrical contact between the thermal interfaces. The cernox sensor is held by the screw that will push the sensor in contact with the surface. A thin layer of Apiezon N grease was used between the sensor and the mounting surface to enhance the thermal contact. The sensor on top was placed between a flat washer and pushed in contact with the surface of the thermal interface by

a screw. The screw was led through a hole in the thermal interface and fastened with a wingnut on the other side.

Figure 3.26: The mechanical holder for the Cernox sensor placed at bottom of the field winding.

Two copper wires were joined with each of the two sensor lead wires. This four-wire configuration is preferred, as it will avoid uncertainties associated with lead resistance when the voltage over the sensor is measured. A copper wire with diameter 0.23mm for voltage measurement and a wire of 0.4mm to lead the current was soldered on the sensor lead. A bigger wire was used to lead the current to reduce the heat dissipated in the wire. The wires were also thermally anchored to assure that the sensor and the leads are at the same temperature as the field winding. This was necessary because the heat flowing through the connecting leads can create an offset between the sensor and the true temperature of the field winding. The wires were soldered with the same Almit solder used in this project.

3.11 Cryostat and Vacuum Pump

The field winding was placed in a cryostat to cool it below 20°K. There are two temperature stages inside the cryostat as the field winding is placed inside a copper shell covered with layers of aluminum foils. The copper shell will be at a temperature of 60-70°K while the field winding will reach down to a temperature below 20°K. Parts of the copper shell is shown in Figure 3.27, as a decagon surrounding the field winding in the middle. Copper plates were placed in front and back of the field winding as well to complete the copper shell. Many layers of aluminum foil and mesh fabric were placed outside the copper to reduce the heat radiation from the cryostat vessel at ambient temperature.

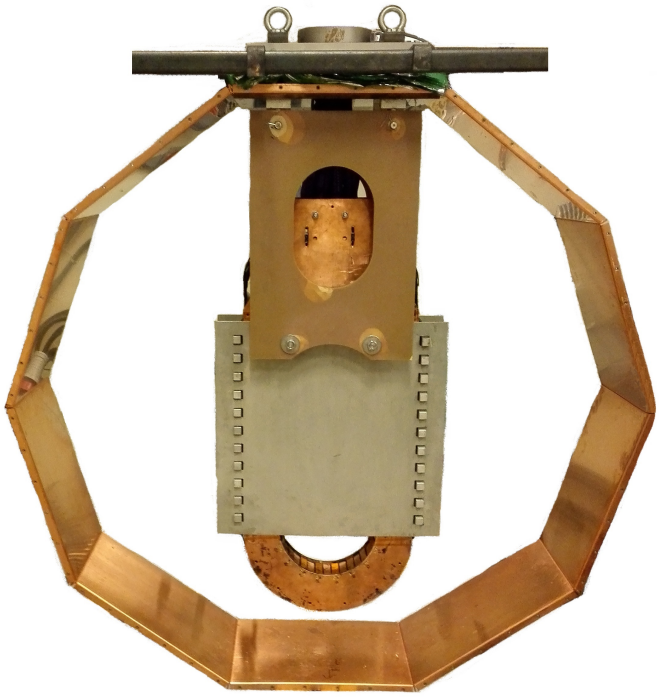

Figure 3.27: The inside of the cryostat with the field winding placed in the middle.

Vacuum was required to minimize the convective heat transfer from the ambient to the field winding. A vacuum system was therefore connected to the cryostat vessel and are shown to the right in Figure 3.28. The system consists of two pumps, one rotary vane pump from Alcatel for pre-vacuum pumping and one turbo molecular high vacuum pump from Pfeiffer. The Alcatel pump was first used to pump the pressure of the vessel down to 100-200 micron, which is about 0.133-0.266mbar.

The turbo molecular pump was then connected in series with the rotary vane pump to get an even lower pressure. The pressure at the end reached down to 0.13µbar, which is more than 99.99% vacuum.

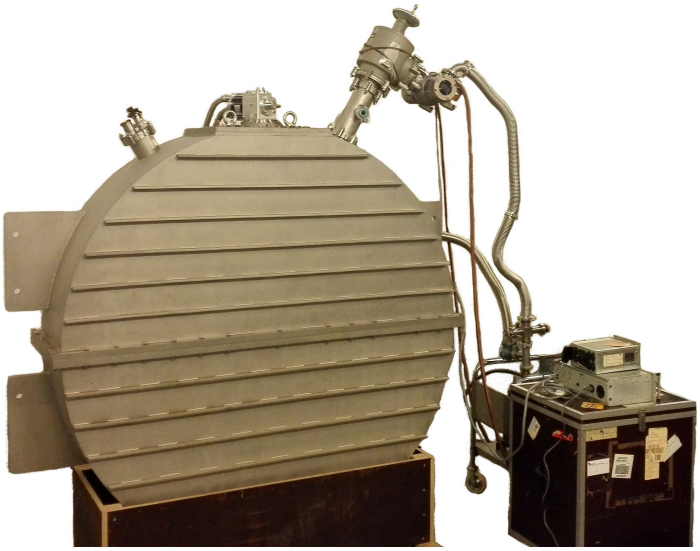

Figure 3.28: The cryostat with vacuum pump and cold head connected.

3.12 Cooling System

The cooling system consist of a cold head connected to a compressor unit, where both components are produced by Sumitomo Heavy Industries. The cold head model is RDK-408S and the compressor model is CSW-71D. The cold head works as a two stage GM cycle cryo-refrigiator with a cooling capacity of 30W at 45°K at the first stage, and 5.4W at 10°K at the second stage. The cold head was connected thermally to the field winding by heat conductors made of thin copper plates bended, as illustrated in Figure 3.29. The heat conductors are bended in a circular shape for flexibility because of the difference between the coefficients of thermal expansion for the materials. The cold head and the copper of the thermal interface will contract differently as the temperature decreases from 300°K to 20°K. These contractions are rather small but need to be taken into account. The flexibility was also helpful while fastening the heat conductors to the field winding and cold head. An extension of the cold head was also made of copper with a high of 13mm. This made it possible to connect the cold head to the field

winding. Apiezon N vacuum grease was used to improve the thermal connection between all the pieces made of copper.

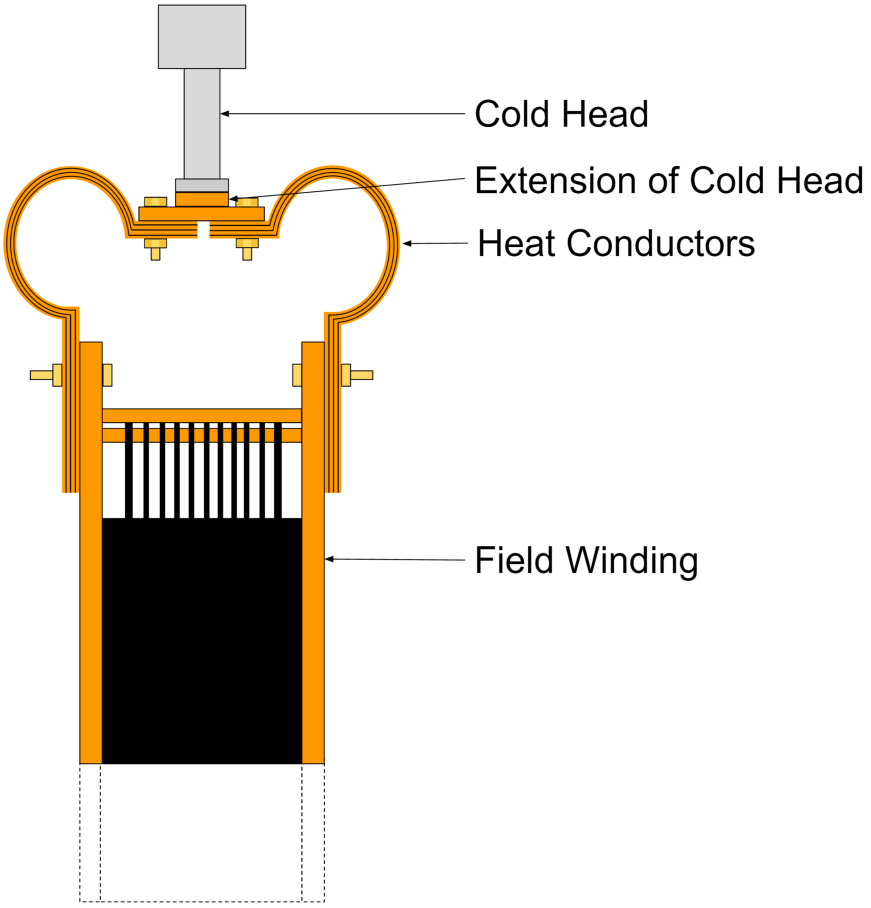

Figure 3.29: Illustration of the thermal connection between the field winding and the cold head. The heat conductors are made of several layers of copper that are bended.

Chapter 4

Simulation of Magnetic Field and Forces

A model of the field winding was made in COMSOL multiphysics to simulate the magnetic field produced and the forces acting on the field winding. COMSOL multiphysics is a simulation software based on the finite element method for finding approximate solutions. The software can model and simulate any physics-based system, and find the solutions for electrical, mechanical, fluid flow and chemical applications [14]. In this project was the software used to simulate the electromagnetic field produced by the field winding in a static application. The total Lorentz force acting on the field finding was also of interest, due to the strength of the mechanical support. The solution for the magnetic field was used to calculate the safety distance from the field winding with respect to ferromagnetic and electronic medical devices sensitive to magnetic fields.

4.1 ICNRIP Guideline for Magnetic Exposure

Electromagnetic interference from low-intensity static fields has been observed to affect the operation of pacemakers and other types of medical electronic devices. The operation of these devices is not adversely affected by static magnetic fields below 0.5 mT [1]. In addition many implanted medical devices contain ferromagnetic materials that can make them susceptible to forces an torque in static magnetic field [1]. The exposure limit of 0.5 mT is a guideline set by the International Commission on Non-Ionizing Radiation Protection (ICNIRP). ICNIRP is an independent organization that provides scientific advice and guidance on health

and environmental effects of non-ionizing radiation to protect people and the environment from detrimental exposure. The guideline is based on number of scientific studies where the possible health effects of exposure to static magnetic fields are look into. The result of the simulation was compared to the 0.5 mT limit to find the safety distance that would not effect implanted medical devices. Guidance for occupational exposure and exposure of the general public is given in Table 4.1. These values are much higher than the restriction level of 0.5 mT for people with implanted medical devices. In comparison is the natural static magnetic field of the Earth 30 to 70 µT depending on the geographic location [1].

Table 4.1: Limits of exposure to static magnetic fields [1].

Exposure characteristics	Magnetic flux density
Occupational	
Exposure of head and of torso	2T
Exposure of limbs	8T
General Public	
Exposure of any part of the body	400 mT

4.2 The Model of the Field Winding

The model made in COMSOL was build in three dimensions to find the safety distance in all direction from the field winding. The geometry of the field winding was constructed in a 20m block of air in all directions. The field winding was placed in the middle, such that the magnetic field could be simulated 10 meter in every direction from the center of the field winding. A Multi-Turn Coil property was added to the domain of the field winding to simulate the current and turns. A Multi-Turn Coil is a lumped model for a bundle of tiny wires tightly wounded together, but separated by an electrical insulator. In this scenario, the current flows only in the direction of the wires and is negligible in other directions.

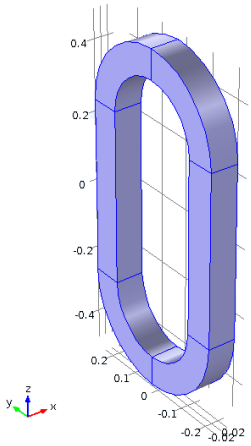

Figure 4.1: The model of the field winding made in COMSOL Multiphysics.

The model was simulated with a current of 200A and 2080 turns, where the geometry and the orientation of the field winding is shown in Figure 4.1. The geometry is simplified but have the same racetrack shape and dimensions as the real field winding. The orientation is also correct with respect to the test setups made for the field winding. The model could be more simplified because of axis symmetry, but this was not done as the simulation time was already relatively short.

4.3 Simulation of Magnetic Field

The result of the simulation is shown in Figure 4.2, where the magnetic field density is plotted with respect to the distance from the center of the field winding. The y axis is made logarithmic as the field decreases very quickly with respect to the distance from the field winding. The plot shows the result for a simulation with a current of 200 A and 2080 turns. The safety limit of 0.5 mT is also plotted as the constant black line. As expected is the field strongest close to the field winding which is represented by the irregularities in the begging of the plots. This is where the plot lines crosses the field winding in Y and Z direction. The magnetic field in the X direction is also decreasing more slowly than the other two direction. This is also expected because of the orientation of the field winding, as it is designed to produce a magnetic field in this direction. The safety distance for this simulation turned out be about 3 m in Y and Z direction and 3,7 m in X direction. A restricted area of 4 m in every direction should therefore be sufficient with a current of 200 A.

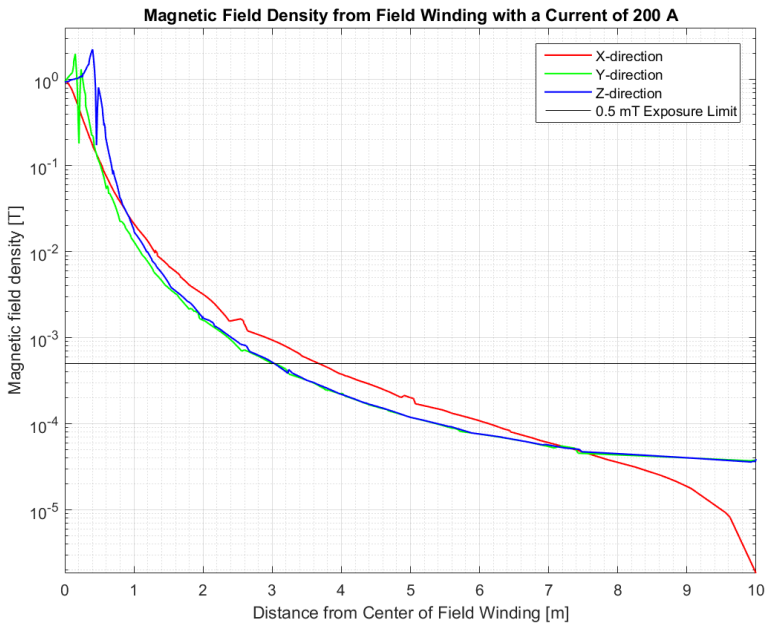

Figure 4.2: The magnetic field density with a current of 200A simulated in the field winding.

The flux lines of the magnetic field is shown in Figure 4.3, and shows the direction of magnetic field in the space. The lines are chopped due to a coarse mesh size of the simulation in air to make the simulation faster. The magnetic field is strongest

at the the inner edge of the field winding and close to zero in the middle of field winding. The average magnetic field in the cross section of the field winding is calculated to 1.2T.

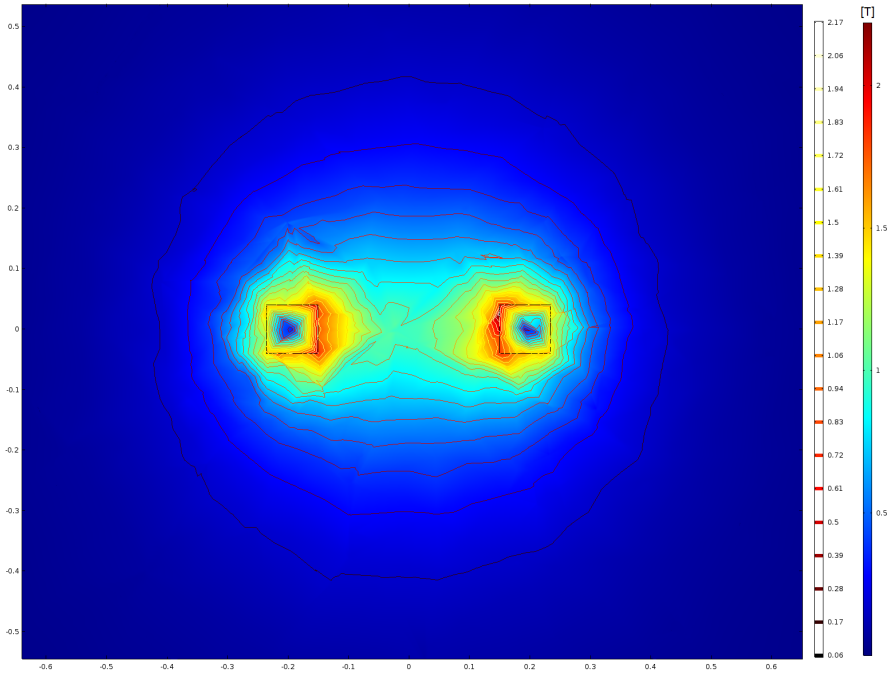

Figure 4.3: Flux lines and field strength of the field winding in the XY-plane.

Since the current and the magnetic field is proportional as given in Equation 2.5, was the safety distance calculated with respect to different magnitudes of the current. This would be useful while testing the field winding, and to find an appropriate location with enough space with regards to safety. Figure 4.4 shows the safety distance in all three direction with respect to the current in the field winding. The plot in Figure 4.4 is the distance where the limit of 0.5 mT occur with respect to the current in the field winding.

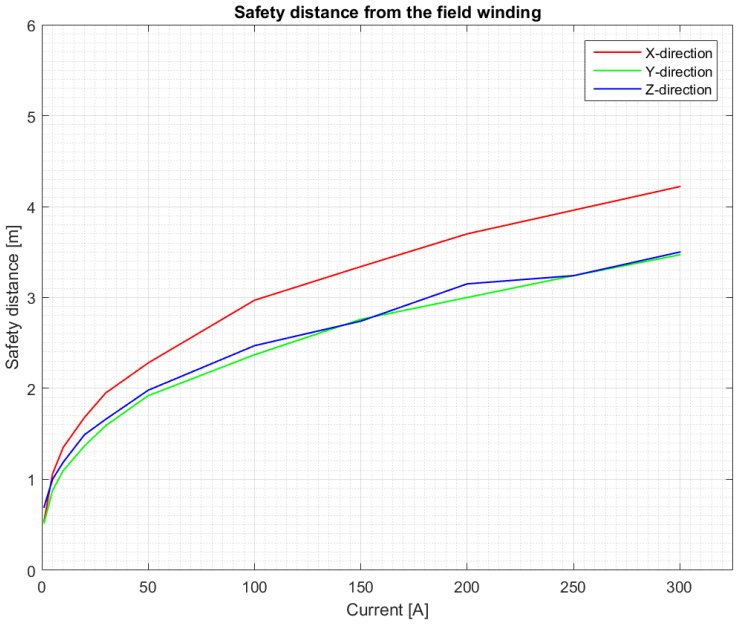

Figure 4.4: The safety distance from the field winding in all three directions.

4.4 Magnetic Force

The field winding is supported by a mechanical support because of the magnetic forces acting on every wire of the winding. These forces together are strong enough to deform the field winding unless the mechanical support are supporting it. The magnetic forces was simulated in a two dimensional model of a cross section of the field winding. The forces on the winding are illustrated in Figure 4.5 by the black arrows representing the force by the size. The surface plot is the magnetic field produced by the two conducting wire. The force was found by adding a force calculation included in COMSOL to the model. The force was calculated by COMSOL to be about 89kN/m on each side of the field winding. This implies a total force of 89kN on the mechanical support as the total length of each straight edge is 2 times 0.5 m.

This force calculation was also done on the straight edges in the 3D model as well. The force calculated pushing each straight edge was about 68kN witch implies a total force of 136kN on the mechanical support. The big difference between the two simulation is caused by the magnetic field. The 3D model gets a much stronger magnetic field because of the contribution of the current in each end where the coil is turning. This gives us a much higher magnetic field overall along the straight

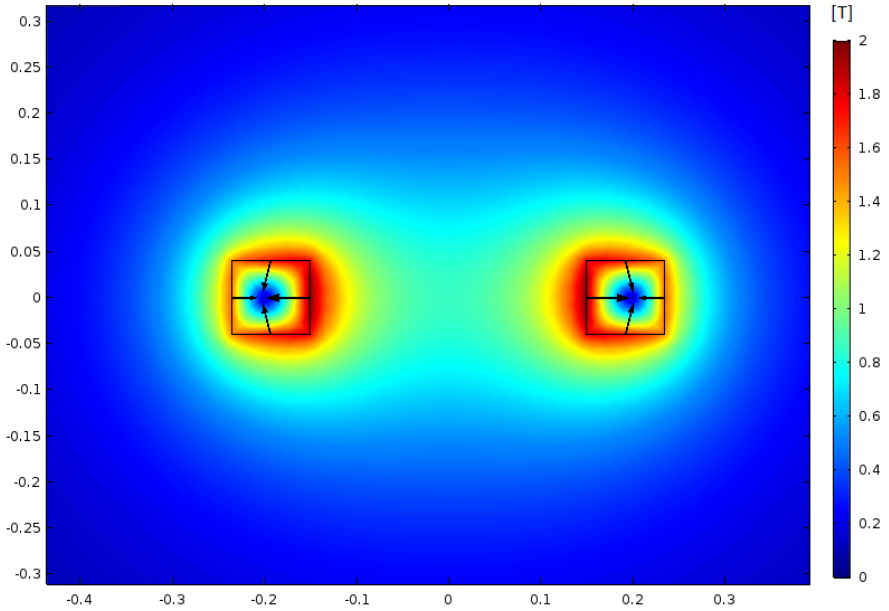

Figure 4.5: The Force and magnetic field of the cross section of the field winding.

edge of the field winding. The simulation compared to the calculation in Equation 3.2, shows that this was an overestimation, with a three times higher force than the 3D simulation. The force in reality will be higher than the force simulated because forces towards the center will act on the turn and contribute to a force bending the field winding outwards. The force simulated here is only the force on the straight edges, but it gives us an idea of how big the force is going to be.

Chapter 5

Testing the Field Winding in Superconductive State

This chapter describes how the testing of the field winding was done and how the measurements was done. The field winding was cooled down below 20°K to verify that all the coils were superconductive and measure the resistance of every joint. The voltages and temperature were measured by the systems described in Chapter 3. The list of equipment is given in Appendix H, where all the equipment used during the project is given.

5.1 Temperature Measurement During Cool Down

The temperature was measured by the two Cernox sensors mounted on the field winding. The results would give an overview of the temperature during cool down, with respect to time and position of the field winding. The result is given as a temperature plot in Chapter 6.1

5.2 Verifying Superconductivity of Every Coil

Superconductivity of every individual coil needs to be verified to be able to test the field winding with high currents up to 200A. The voltage over every coil was measured while different currents up to 16A were flowing through the field winding. An increased voltage over the coil when the current was increased, would imply a defect coil that are not superconductive. A constant and stable current was

also very important to avoid measuring the inductive voltage made by the large inductance of the coils. It was therefore important to make sure that the current was stabilized such that the measurements would be correct. It turned out to be rather difficult to get a constant current with the power supply only connected to the field winding. A resistance in series with the field winding was therefore connected to make sure that the current was stabilized.

5.3 Measure the Resistance of the Joints

The resistance of every joints was calculated by voltage measurements to validate their quality. It is important to know the resistance of every joint, such that the power dissipated in the joints could be calculated at higher currents. The voltages over the joints were measured at the same time as the individual coils were tested.

5.4 Measuring the Inductance

The inductance of the field winding was found by ramping up the current with an almost constant voltage. This makes it possible to calculate and find an estimation of the inductance. The resistance connected in series with the field winding was removed to minimize the resistive voltage drop such that the voltage would only increase the current in the field winding. A small resistance in the cables leading the current to the field winding was not possible to eliminate.

The inductance was calculated by using Equation 2.8. The relationship between self-inductance, voltage and current through a circuit is given and the equation can be rewritten to find the inductance.

$$V = L\frac{di}{dt} \longrightarrow L = V\frac{dt}{di} \tag{5.1}$$

5.5 Datalogging

All the measurements were logged by an Agilent 34970A data logger and collected by a computer with the BenchLink Data Logger 3 software. This software provides a convenient way to collect and analyze the data by having a continuous plotting of the measurements while testing. The system for voltage measurements is given in Appendix F, where all the channels on the plug-in modules are listed. The

current through the Cernox sensors were logged by one of the current channels on the plug-in module for the data logger. The current of the field winding was logged by measuring the voltage over a shunt connected in series with the field winding. The ratio between the current and voltage was 600 such that a gain of this size was configured in Benchlink. This made it possible to log the current of the field winding and watch it live on the screen.

Chapter 6

Results

The results of the tests described in Chapter 5 are presented in this chapter.

6.1 Temperature During Cool Down

The temperature was measured every ten minutes during cool down, and reached a stable low temperature after about 130 hours. The minimum temperatures measured by the two Cernox sensors were 18.9°K and 17.7°K, where the lowest temperature was measured at the bottom of the field winding.

Figure 6.1 shows the temperature measurements from the two Cernox sensors from the beginning. The temperature was found by measuring the resistance of the Cernox sensors and comparing it with the calibration data given for each sensor. Linear interpolation was used to estimate the exact temperature of the field winding as the calibration data were given in tables.

As expected was the temperature lower at the top of the field winding during cool down. This happened because the heat uses longer time to be transferred to the cold head from the bottom of the field winding than from the top. However, at the end of the cool down became the temperature at the bottom of the field winding about 1°K lower than at the top. This could be explained by the heat transfered by the voltage measuring system. These wires transfer heat to the area where the top sensor is mounted, and would probably increase the temperature.

The temperature did not go down as low as first expected. An earlier project completed in 2009 [11], measured a temperature as low as 7.4°K. It was expected to get a temperature closer to this result.

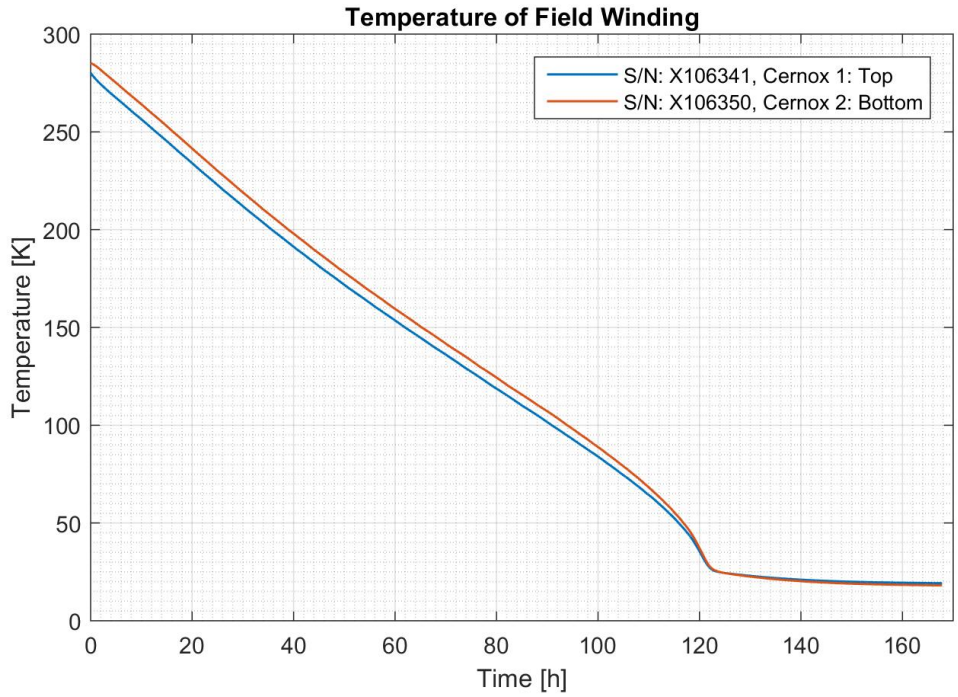

Figure 6.1: The temperature of the field winding during cool down. The field winding was cold enough to start testing after six days.

6.2 Superconductivity

Superconductivity was confirmed for seven out of ten coils in the field winding. Figure 6.2 shows the voltage drop over each coil with respect to an increasing current. The voltage is calculated as the average of 15 measurements over a period of 3.75 minutes, when the current was stabilized to a constant level. The average measurements given without any current flowing through the field winding was subtracted from all the other calculations to compensate the offset values. The current was increased in steps of random size between 3-4A, up to 16A as the highest current tested. Figure 6.2 shows that Coil 1,6 and 10 are not superconductive as the voltage increases with a higher current. The other seven coils looks to be working as they should with no changes in the voltage as the current increases. The resistance of the three defect coils was calculated to be 2.01, 1.91 and 3.40 $\mu\Omega$ by calculating the slope of the plots. The total resistance of the field winding would be around 7$\mu\Omega$ which would dissipate a heat of 0.3W at 200A. This calculation is based on a linear relationship between the current and voltage of the coil. The plot from Figure 6.2 shows a different trend as the relation looks like

a second polynomial function. This means that the resistance increases with an increased current, and more heat will be dissipated. This heat would potentially lead to quenches while testing with higher currents and it was therefore not tested with any higher currents without a quench protection system.

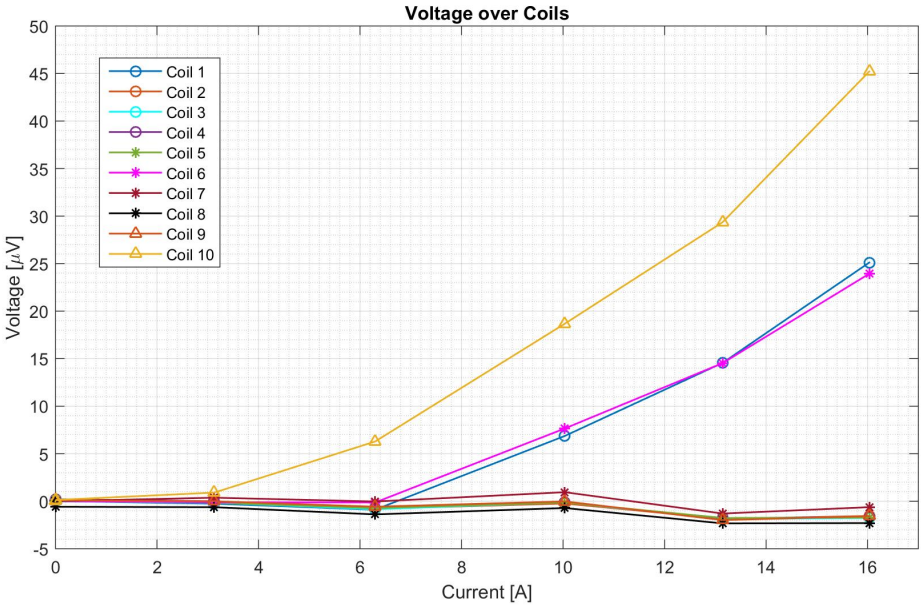

Figure 6.2: The voltage measurements over every individual coil with increased current.

The voltage over the BSSCO HTSs were also measured to verify superconductivity. The same procedure was done to calculate the voltages, and the voltages are presented in the plot in Figure 6.3. The plot shows a linear relationship between the voltage and current, meaning that the BSSCO wires are not superconductive. The slope of the plots gives a resistance of 640 $\mu\Omega$ for the wires placed outside, and 692$\mu\Omega$ for the wires inside. It is assumed that half of the current is flowing through each side when calculating the resistance. A reason for the high resistance might be that the temperature of the first stage is much higher than expected. The BSSCO superconductor have a critical temperature of 110°K, which means that the copper shell might have a higher temperature than this. Since there is no temperature sensor mounted on the copper, is it not possible to say if this is the case. The BSSCO wires could have also been damaged by the heat during soldering or by mechanical stress during assembly. Improvements are required to make sure that the BSSCO wires becomes superconductive, such that the field winding can be tested with currents up to 200A.

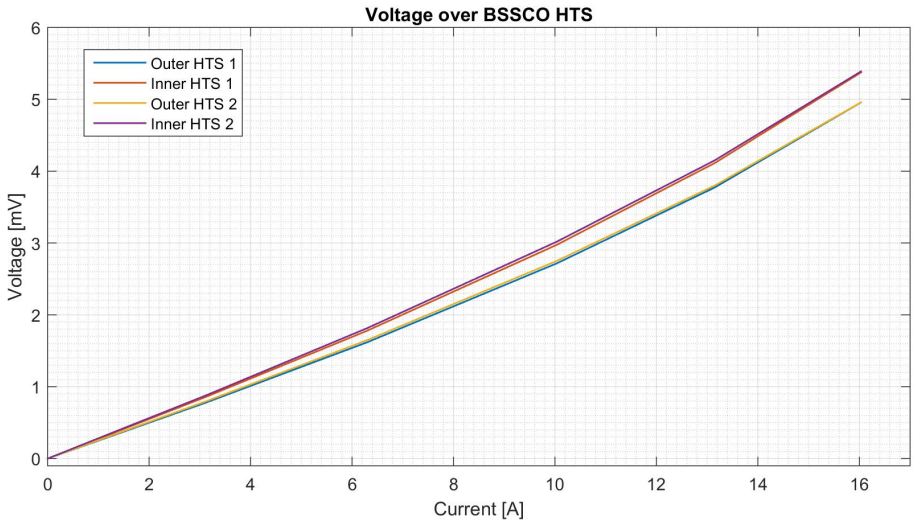

Figure 6.3: The Voltage over The BSSCO HTS.

6.3 Joints

The quality of the joint was tested by measuring the resistance through voltage measurements. It was important to check if the joints were good enough for the field winding to be tested with 200A. The offset value was subtracted from every measurement, but might be wrong due to noise, as the voltages are small and hard to measure. The resistance was therefore calculated from the slope of the measurements from 3 to 16A, where there is a clear linear trend for every joint as seen in Figure 3.5. Joint 8 stands out with a higher resistance than the other joints. There were no problems during the soldering of this joint, and the resistance was calculated to be 110nΩ. The other nine joints have a resistance of 25-43nΩ which is very good.

The results from the measurement of the joints between the BSCCO and MgB_2 are plotted in Figure 6.5. The measurement from the outer joint showed a linear trend, while measurements for the inner joints did not. Especially the measurements from inner joint 2 were not very good, by not having a linear trend of the voltage. It is possible that the voltage over the inner joints became to low and more exposed for noise. The resistance calculated for the joints by assuming half of the current is going true each path is 40-60 nΩ for the outer joints and 8-16 nΩ for the inner joints. These numbers are probably not correct as the current is probably not divided correctly. But it gives an idea that the joints are still good enough.

The total resistance given by the joints in the field winding turned out to be 361

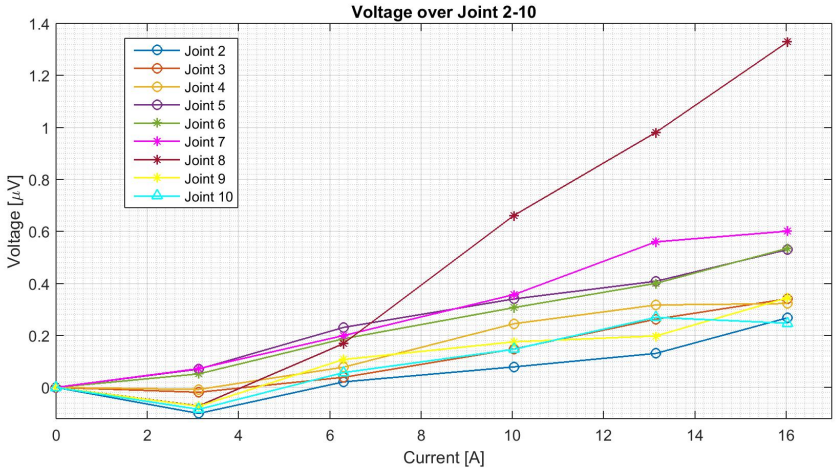

Figure 6.4: The voltage over joint 2-10 during the test with different currents

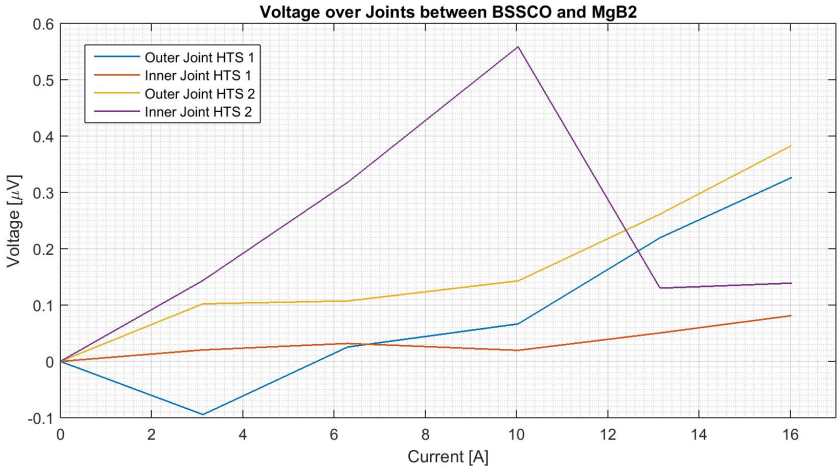

Figure 6.5: The voltage over each joint between BSSCO and MgB_2 superconductors during test with different currents

nΩ for the MgB_2 joints. The total resistance for the HTS joints were a little harder to calculate as these joints are in parallel. Since the currents are not know in each path is it hard to know for sure what the resistance is. With a current divided equally is the total resistance added together 65 nΩ. At 200A will the MgB_2 joints dissipate 14.44 mW with an average of 1.6 mW for each joint. This dissipated heat should be low enough to make sure that the joints are kept colder than the critical temperature while testing.

6.4 Inductance

The inductance was found by using equation 2.8, and the measurement from the plot in Figure 6.6. The current and voltage was measured every other second for about 6 minutes. The current ramps up slowly as the voltage of 50 mV was applied to the field winding. The voltage over the field winding gets lower with an increased current due the the resistance in the cables. Two different approaches were used to calculate the inductance because of the resistance in the circuit. The first method compared the measurements between every other second and calculated the inductance. The average of all these calculation gave an inductance of 4.57H. This was done since the voltage could be approximated to be constant over the time period. The second method compared the measurements at 50 and 300 seconds. The voltage was integrated with respect to time and divided by the difference of the current. This calculation gave an inductance of 4.62H.

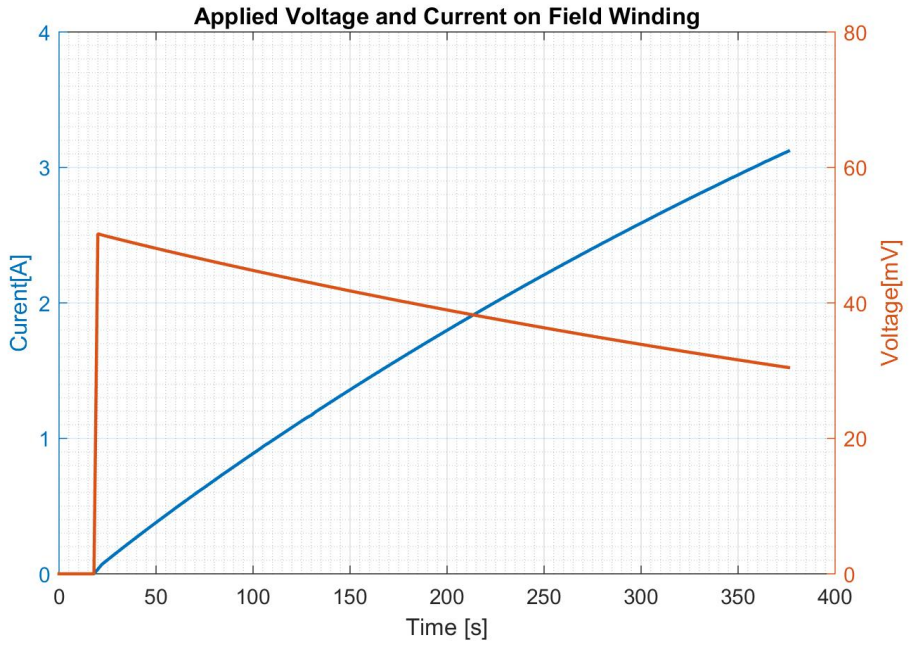

Figure 6.6: The ramp-up current and voltage the the field winding for calculating the inductance.

6.5 Shorting

A second inductance test was started with 150mV applied, when the field winding suddenly became shorted. The current jumped instantly to the current limitation set by the power supply. This made it impossible to test the field winding without opening the cryostat and fix the shortening. After some troubleshooting was it concluded that the current could not go through the field winding, because a voltage over the HTSs was only measured on one side of the field winding. Since the current also jumped from one level to the next, would also imply a low inductance path for the current. It was therefore assumed that the field winding was still working as it should, but there was a shortening somewhere in the circuit. No further tests were conducted in this project due to the shortening and limited time.

Chapter 7

Discussion

This master thesis discusses the testing and assembly of a superconductive field winding.

The assembly of the field winding was more time consuming than first expected. A lot of small things added up to take a lot of time. One of the things that should have been done differently was to use kapton tape between the first coil and the copper teeth. The consequence of this was an electrical connection between the thermal interface and the field winding. This could have led to the shorting described in Chapter 6.5. The location of the joints could have been closer to the field winding as well. This made it impossible to use two of the fastening holes for the heat conductors as the cooling pieces for the joints were blocking the holes. This might not be a big problem, but still a thing that could have been done differently. All the other problems that occurred during the assembly were solved the best way possible. The mechanical support was designed perfectly for the field winding, but the assembly was a little challenging. Since the mechanical support was supposed to be as tight as possible, was it forced together by using tensioning straps when it was placed around the field winding.

The time for testing the field winding was limited at the end of the project, and there was no time to improve and test the field winding a second time. The minimum temperature was 10°K more than expected, because a temperature of 7.4°K was reached in a similar project conducted in 2009 [11]. 17.7°K was the lowest temperature measured in the cryostat by the Cernox sensor placed at the bottom of the field winding. It is possible that the temperature of the high temperature stage is much higher than expected. This would make it harder to cool down the field winding as more radiation from the copper shell will heat it up. This statement also agrees well with the BSSCO HTS not entering superconductive

state. The thermal connection between the copper shell and the cold head was never checked and might be the reason for the high temperature. The thermal connection between the cold head and thermal interface should also be checked. The fastening between the cold head and the heat conductors should be improved by adapting it better and make it more flexible. Bigger screws and nuts should be used to fasten the cold head, as the small nuts were hard to tighten. More temperature sensors should be installed, and especially one at the copper shell. These sensors could be thermocouples to reduce the cost. These sensor do not have to be very accurate but must be able to tell if the temperature is 110°K or 60°K. The sensors should give an idea of how the temperature is distributed around the cryostat.

The thermal anchoring of the wires measuring the voltage should also be improved. This was done only by attaching them to the copper shell by two screws with spacers. This should be done properly to make sure more of the heat conducted by the wires is removed by the high temperature stage of the cold head. The heat transported by the wires to the field winding could be the reason that the Cernox sensor placed next to the terminal strips measured a temperature of 1°K higher than at the bottom. The thermal anchoring of the wires to the cernox sensors should also be improved to be sure that there are no offset created between the sensor and the true temperature of the field winding.

The BSCCO HTSs are not entering the superconducting state most likely because of the temperature not being low enough at the high temperature stage. It is not suspected that the wires are damaged mechanically, as they were treated carefully during the assembly. No temperature sensors were installed at the the high temperature stage to confirm this, but since the temperature of the second stage became 10°K higher than expected, is it possible that this is the problem. Tubes connected to the field winding could be installed around the HTSs to protect the wires from thermal radiation and be sure that the HTSs are cold enough.

The possible high temperature of the HTSs might have had an influence of the two coils at each end of the field winding. Coil 1 and 10 are not confirmed to be superconductive probably because of the temperature. If the highest temperature of the HTSs are above 110°K, is it most likely conducting a lot of heat to the MgB_2 coils. This could increase the temperature above 39°K. The two coils should be tested again with improved thermal connection from the high temperature stage of the cold head to the copper shell.

The resistance in coil 6 is most likely due to a damaged or defect superconductor. Since the coils on each side of coil 6 are superconductive should the temperature be low enough for coil 6 as well. This coil should therefore be shorted by connecting

coil 5 and 7 together. This could be done by cutting the wires from coil 6 and solder the two joints together to join coil 5 and 7.

The resistance of the joints is low enough to be able to test the field winding with 200A. The average resistance of a joint is 40nΩ. Joint 8 stands out with a higher resistance than the other joints, as it was calculated to be 110nΩ. This is 2.5 higher than the average resistance in the joints. Joint 8 are still acceptable and would be dissipating 4.4mW at 200A. The total heat dissipated in the MgB_2 joints while testing with 200A will be 15mW. The measurements from the joints between BSCCO and the MgB_2 superconductors were of lower quality than the MgB_2 joints. This is most likely because the joints are in parallel. The measurements did not show any extremely high voltages and since the other joints have such low resistance should these joints also be good. All the joints are made by the same procedure, such that the quality should be good enough between the BSCCO and MgB_2 superconductors as well.

The inductance was calculated to be around 4.6H, which is close to what J.C. Eliassen measured in room temperature in his project [7]. This would imply that the turn to turn insulation works as it should, since the current is flowing true the hole field winding during ramp up. This test proves the insulation ability of the epoxy to be sufficient during ramp up of with 50mV applied to the field winding. With this voltage would 200A take 5 hours to reach. The field winding should therefore be tested with a higher voltage to see if the ramp up of the current could be done any faster. This was not done due to the shortening.

Chapter 8

Conclusion

The minimum temperature of the field winding was 17.7°K, measured by the Cernox sensor placed at the bottom of the field winding. This was 10°K higher than expected, and might be caused by a poor thermal connection between the cold head and the copper shell. The temperature of the copper shell in the cryostat should be measured to verify if this temperature is to high.

3 out of 10 individual coil did not become superconductive. The temperature in Coil 1 and 10 might have been to high, as parts of the BSCCO HTS were not colder than 110°K. Improvements should be done to the cooling of the high temperature stage before concluding Coil 1 and 10 to be defect. Coil 6 is assumed defect as both coils next to it are superconductive, such that the temperature should not be a problem for coil 6. The coil should be shorted to be able to test the field winding with 200A.

The BSCCO HTS wires were not superconductive during the testing. This is most likely due to a high temperature of the copper shell. This could also effected Coil 1 and 10. A temperature sensor should be placed on the high temperature stage before the next test to confirm the temperature.

The joints are good, with a low enough resistance to test the field winding with 200A. The soldering technique is concluded to be good as the average resistance of the joints are 40nΩ. The total heat dissipated in the joints would be around 15 mW at 200A.

The inductance was measured to be around 4.6H. This corresponds well with the measurements made in a previous project done by J.C Eliassen in room temperature [7]. This would imply that the current is flowing trough the whole field winding, such that the turn to turn insulation works as it should. The wet wind-

ing technique is therefore concluded to work adequately because the turns are insulated.

The reason for the shorting of the field winding was not determined. The cryostat should be opened and the wires should be checked for faults. This was not done due to time limitation.

Chapter 9

Recommendation for Further Work

Further work should consist of making the field winding work in superconductive state. A better and more practical solution to attach the cold head to the thermal interface should be found. Bigger screws and nuts should be used to be able to fasten the cold head better to the thermal interface. The connection between the high temperature stage of the cold head and the copper shell should be investigated to see if there is a bad thermal connection. This bad connection could have led to a higher temperature than expected during testing and probably be the reason why the HTSs, coil 1 and 10 were not superconductive. Coil 6 should be shorted as it is most likely defect, when not being superconductive at a temperature of 18°K.

A quench protection system should be designed to be able to test the field winding with higher currents than 16A. This system should cut the power supply if parts of the field winding should suddenly not be superconductive. The amount of energy in the coil should be dissipated in a resistance connected in parallel to the field winding.

The field winding should be tested with a current up to 200A as soon as it works perfectly in superconductive state and a quench protection system is installed. The magnetic field should be measured to see if the the field winding could be used in a generator. The magnetic field could also be compared to the simulation done in COMSOL Multiphysics, to check the reliability of the simulation. The field winding should also be tested in an alternating magnetic environment that would simulate the stator current in a generator. The performance of the superconducting field winding should be measured to see if it is affected by the alternating magnetic

field. At the end, should the maximum performance of the field winding be tested by ramping the current up to the critical current. This would probably be the last test of the field winding and destroy it.

Bibliography

[1] ICNIRP. Guidelines on limits of exposure to static magnetic fields. 2009.

[2] R.G. Sharma. *Superconductivity: Basics and Applications to Magnets*. Springer International Publishing, 2015.

[3] A star Maths and Physics. The Meissner Effect. http://astarmathsandphysics.com/a-level-physics-notes/168-electricity/2605-the-meissner-effect.html. Retrieved December 2015.

[4] Columbus Superconductor. Wire Proposal. Power point slides recieved on mail from Niklas Magnusson. 20.05.2016.

[5] Sumitomo Electric Superconductor. BSCCO Specifications. http://global-sei.com/super/hts$_e$/$type_h t.html. Retrieved May$2016.

[6] A.B. Abrahamsen A. Nysveen J. Bjerkli M. Runde N. Magnusson, J.C. Eliassen and P. King. Design aspect on winding of a mgb2 superconducting generator coil. 2015.

[7] J.C. Eliassen. Winding and testing of superconducting coils. 2015.

[8] Science Educators from NSTA. The History of Superconductors. http://www.superconductors.org/history.htm. Retrieved December 2015.

[9] Alan Chodos, APS. April 1911: Onnes Begins work on Superconductivity. https://www.aps.org/publications/apsnews/200704/history.cfm. Retrieved December 2015.

[10] King-Ning Tu. *Solder Joint Technology: Materials, Properties, and Reliability*. Springer New York, 2007.

[11] E. Engebrethsen. Testing av superledende spoler. 2009.

[12] M. Paulsen. Soldering techniques for mgb2 superconductors. 2015.

[13] INCO Limited. Materials for cryogenic service: Engineering propoerties of austenitic stainless steels. 1974.

[14] COMSOL. Multiphysics Software. https://www.comsol.no/products. Retrieved May 2016.

Appendix A

Heat profile of the soldering

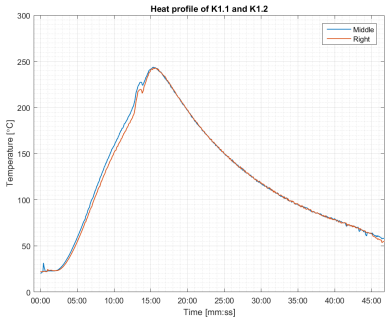

Figure A.1: First soldering between copper termination and BSCCO HTS.

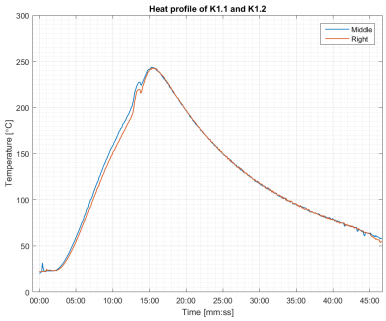

Figure A.2: Second soldering between copper termination and BSCCO HTS.

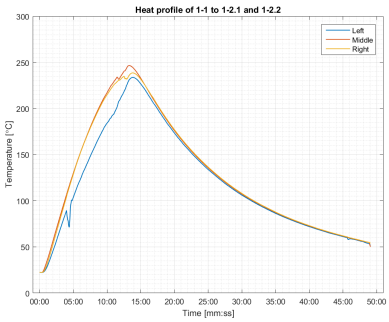

Figure A.3: First soldering between BSCCO HTS and MgB_2

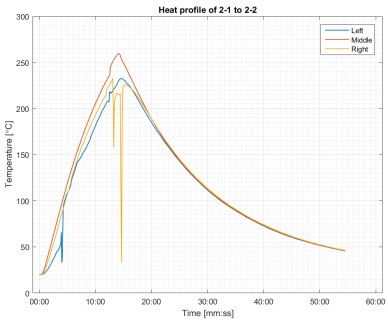

Figure A.4: Soldering between Coil 1 and 2.

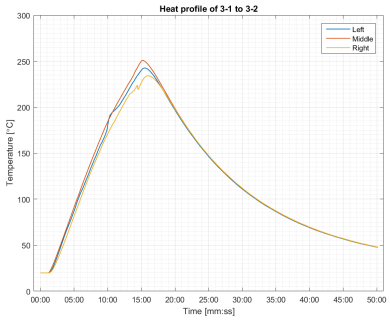

Figure A.5: Soldering between Coil 2 and 3.

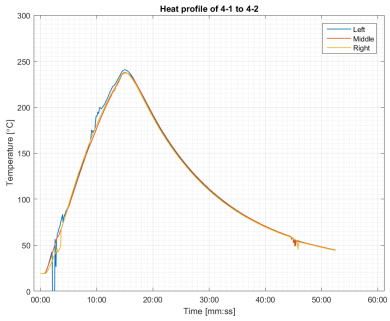

Figure A.6: Soldering between Coil 3 and 4.

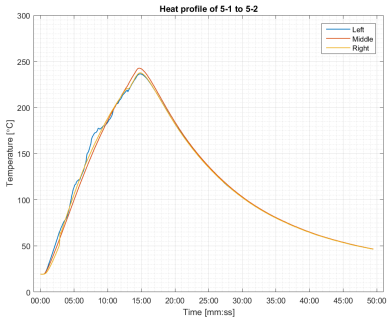

Figure A.7: Soldering between Coil 4 and 5.

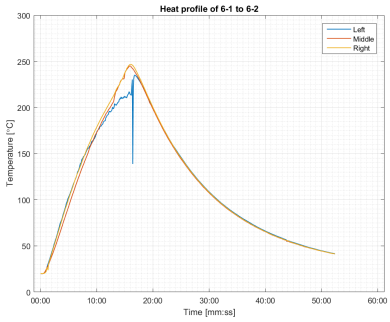

Figure A.8: Soldering between Coil 5 and 6.

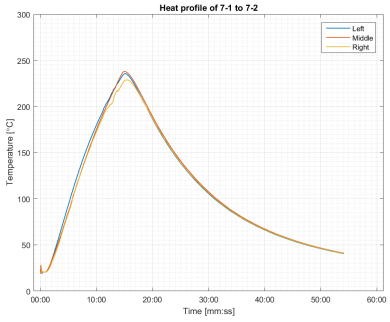

Figure A.9: Soldering between Coil 6 and 7.

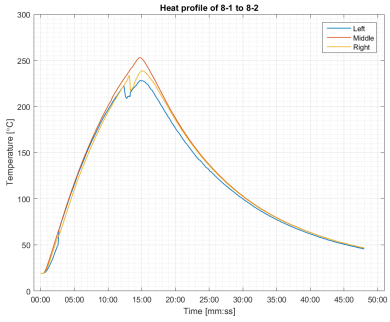

Figure A.10: Soldering between Coil 7 and 8.

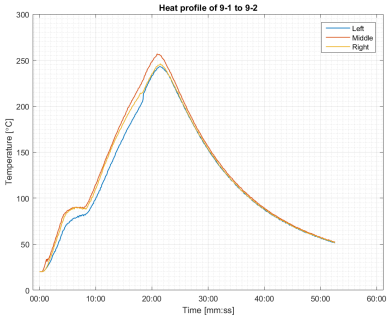

Figure A.11: Soldering between Coil 8 and 9.

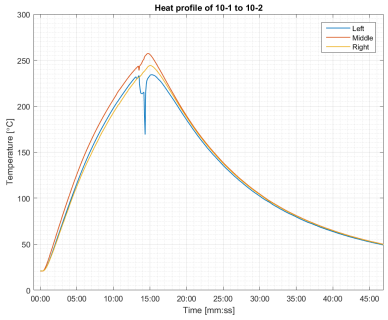

Figure A.12: Soldering between Coil 9 and 10.

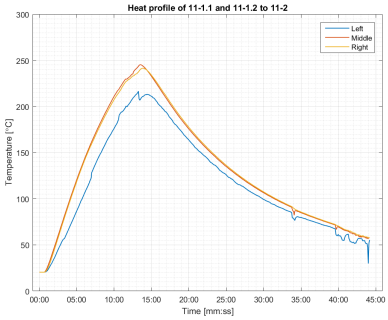

Figure A.13: Second soldering between BSCCO HTS and MgB_2 superconductor.

Appendix B

Design of cooling pieces for joints

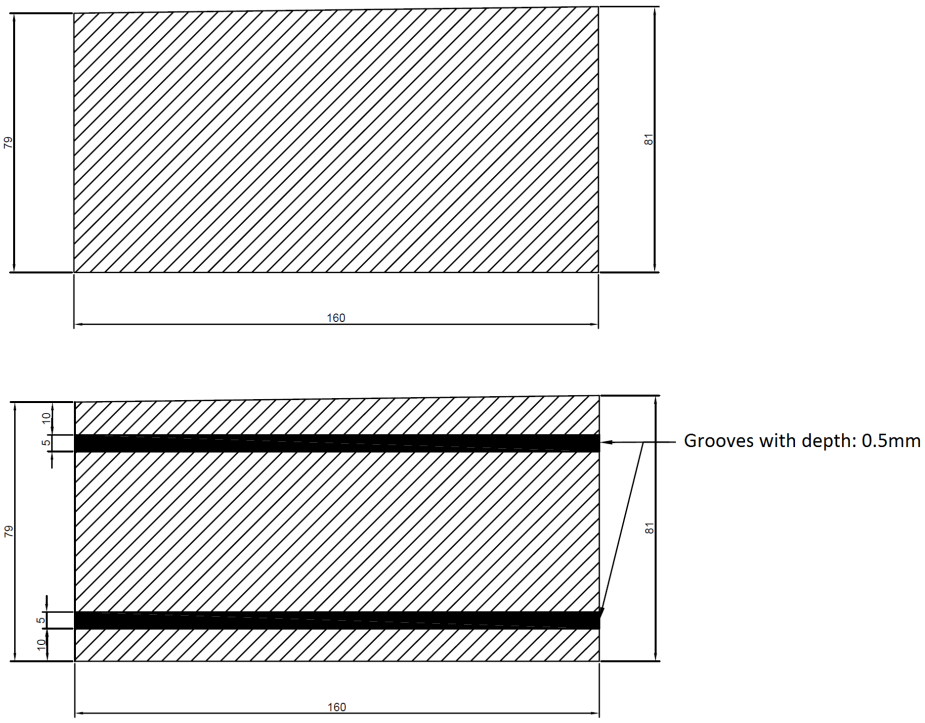

Figure B.1: Dimensions of the copper pieces for cooling the joints. The unit is millimeter.

Appendix C

Design of the mold for casting parallel surfaces

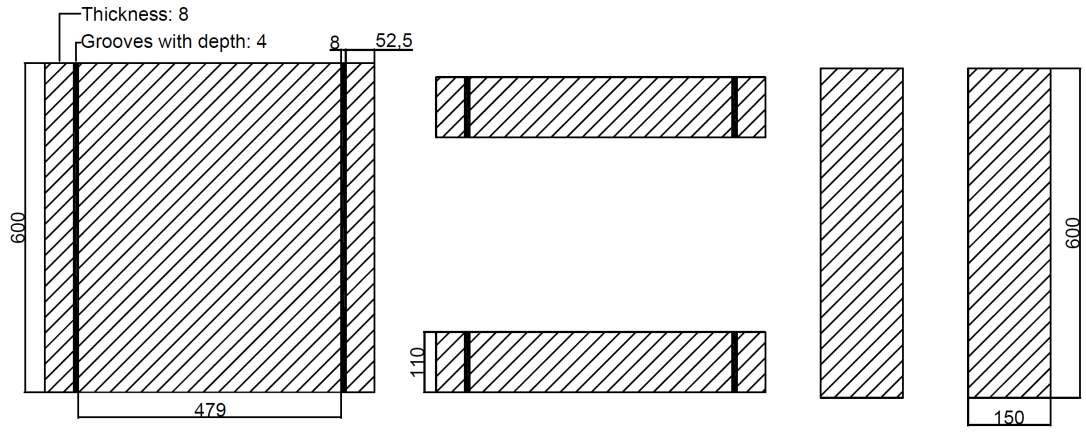

Figure C.1: Design and dimensions of the mold in millimeter

Appendix D

Mechanical support

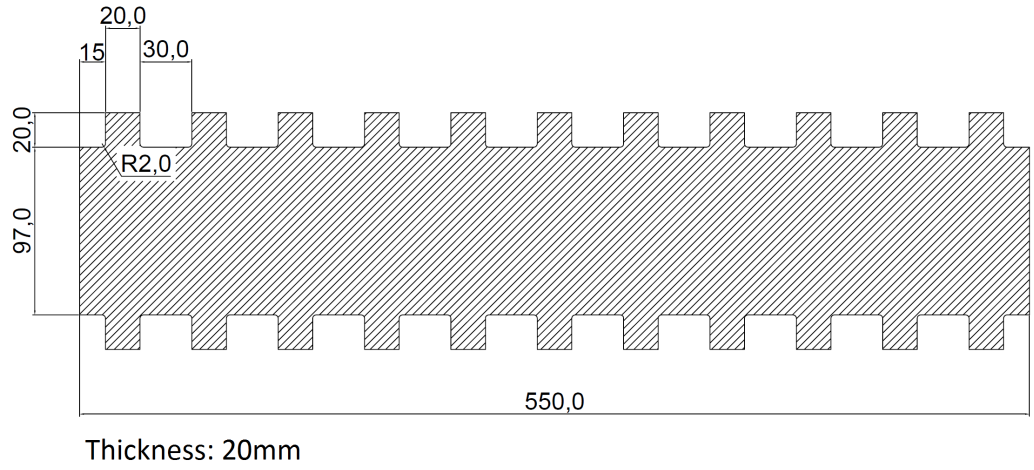

Figure D.1: Dimensions of the side of the mechanical support in millimeter

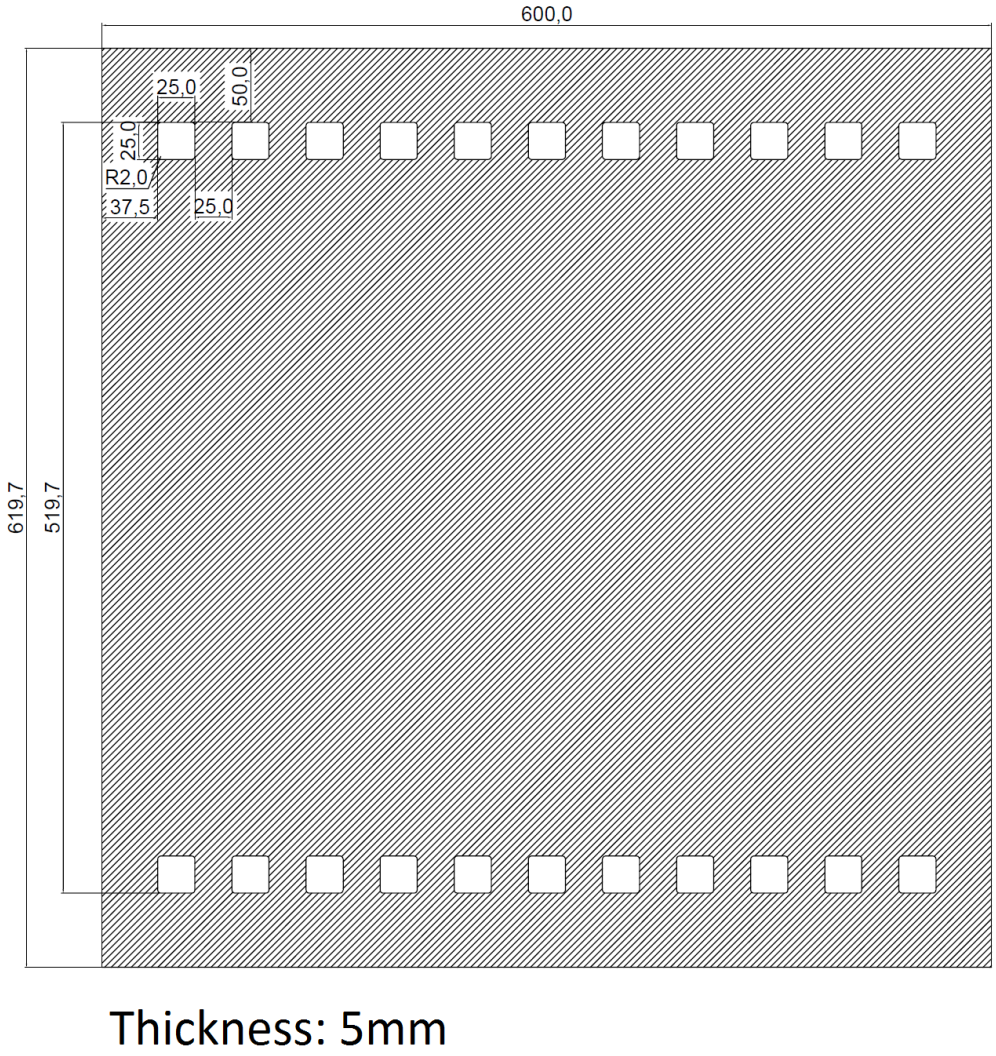

Figure D.2: Dimensions of the top of the mechanical support in millimeter

Appendix E

Copper termination

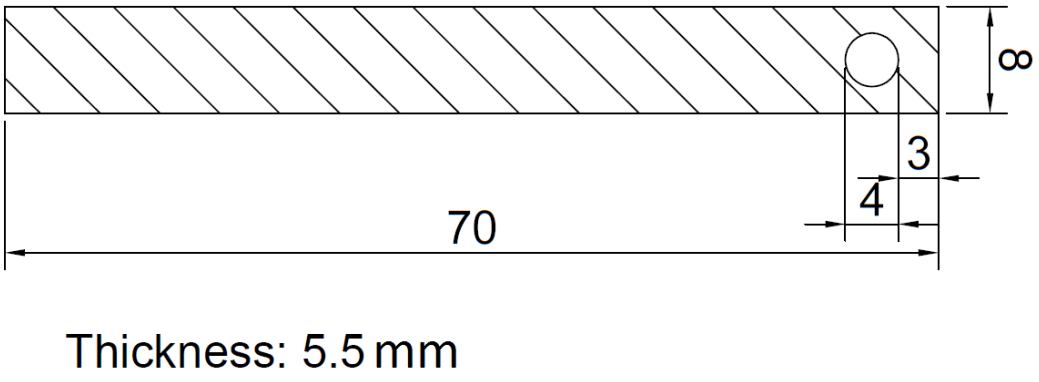

Figure E.1: Dimensions of the copper termination in millimeter

Appendix F

System for Voltage measurement

Table F.1: System for Voltage measurements

Location/function	Enameled copper marked with:	Number d-sub	Color on isolation of wire inside cryostat	D-sub number	Color on isolation of wire outside cryostat	Channel multiplexer	Multiplexer card
Voltage HTS at copper termination Outer	K1.1	1	Black	1	Brown	1H	G05-0183-01
Voltage HTS at copper termination Inner	K1.2	2	White	1	Red	2H	G05-0183-01
Voltage HTS at Coil 1 Outer	1-1.1	3	Brown	1	Orange	1L	G05-0183-01
Voltage HTS at Coil 1 Outer		3				3H	G05-0183-01
Voltage HTS at Coil 1 Inner	1-1.2	4	Red	1	Pink	2L	G05-0183-01
Voltage HTS at Coil 1 Inner		4				4H	G05-0183-01
Voltage Coil1 at HTS	1-2	5	Purple	1	Yellow	3L	G05-0183-01
Voltage Coil1 at HTS		5				4L	G05-0183-01
Coil 1		5		1		5H	G05-0183-01
Coil 1		6		1		5L	G05-0183-01
Voltage Joint 2, position 1	2-1	6	Blue	1	Green	6H	G05-0183-01
Voltage Joint 2, position 2	2-2	7	Yellow	1	Turquoise	6L	G05-0183-01
Coil 2		7				7H	G05-0183-01
Coil 2		8				7L	G05-0183-01
Voltage Joint 3, position 1	3-1	8	Green	1	Blue	8H	G05-0183-01
Voltage Joint 3, position 2	3-2	9	Pink	1	Light Blue	8L	G05-0183-01
Coil 3		9				9H	G05-0183-01
Coil 3		10				9L	G05-0183-01
Voltage Joint 4, position 1	4-1	10	Grey	1	Purple	10H	G05-0183-01
Voltage Joint 4, position 2	4-2	11	Brown with green marks	1	Grey	10L	G05-0183-01
Coil 4		11				11H	G05-0183-01
Coil 4		12				11L	G05-0183-01
Voltage Joint 5, position 1	5-1	12	White with green marks	1	White	12H	G05-0183-01
Voltage Joint 5, position 2	5-2	13	Red with blue marks	1	Black	12L	G05-0183-01
Coil 5		13				13H	G05-0183-01
Coil 5		14				13L	G05-0183-01
Voltage Joint 6, position 1	6-1	14	White with yellow marks	1	Brown with black marks	14H	G05-0183-01
Voltage Joint 6, position 2	6-1	15	Yellow with brown marks	1	Red with black marks	14L	G05-0183-01
Coil 6		15				15H	G05-0183-01
Coil 6		16				15L	G05-0183-01
Voltage Joint 7, position 1	7-1	16	Grey with brown marks	1	Orange with black marks	16H	G05-0183-01
Voltage Joint 7, position 2	7-2	17	White with grey marks	1	Pink with black marks	16L	G05-0183-01
Coil 7		17				17H	G05-0183-01
Coil 7		18				17L	G05-0183-01
Voltage Joint 8, position 1	8-1	18	White with pink marks	1	Yellow with black marks	18H	G05-0183-01
Voltage Joint 8, position 2	8-2	19	Pink with brown marks	1	Green with black marks	18L	G05-0183-01

Coil 8		19				19H	G05-0183-01
Coil 8		20				19L	G05-0183-01
Voltage Joint 9, position 1	9-1	20	White with blue marks	1		20H	G05-0183-01
Voltage Joint 9, position 2	9-2	21	Brown with blue marks	1		20L	G05-0183-01
Coil 9		21				1H	G05-0138-01
Coil 9		22				1L	G05-0138-01
Voltage Joint 10, position 1	10-1	22	White with red marks	1		2H	G05-0138-01
Voltage Joint 10, position 2	10-2	23	Brown with red marks	1		2L	G05-0138-01
Coil 10		23				3H	G05-0138-01
Coil 10		24				3L	G05-0138-01
Voltage Coil10 at HTS	11-1	24	White with black marks	1		4H	G05-0138-01
Voltage Coil10 at HTS		24				5H	G05-0138-01
Voltage HTS at Coil 1 Outer	11-2.1	25	Grey with pink marks	1		4L	G05-0138-01
Voltage HTS at Coil 1 Outer		25				6H	G05-0138-01
Voltage HTS at Coil 10 Inner	11-2.2	1	Black	2	Brown	5L	G05-0138-01
Voltage HTS at Coil 10 Inner		1				7H	G05-0138-01
Voltage HTS at Copper termination Outer	K2.1	2	White	2	Red	6L	G05-0138-01
Voltage HTS at Copper termination Inner	K2.2	3	Brown	2	Orange	7L	G05-0138-01
Cernox Current +	CX_C+	4	Red	2	Pink	21I	G05-0138-01
Cernox Current -	CX_C-	5	Purple	2	Yellow	21L	G05-0138-01
Cernox 1 Voltage +	CX1_V+	6	Blue	2	Green	9H	G05-0138-01
Cernox 1 Voltage -	CX1_V-	7	Yellow	2	Turquoise	9L	G05-0138-01
Cernox 2 Voltage +	CX2_V+	8	Green	2	Blue	10H	G05-0138-01
Cernox 2 Voltage -	CX2_V-	9	Pink	2	Light Blue	10L	G05-0138-01

Appendix G

Thermal Conductivity of Wires for Voltage Measurement

Table G.1: Thermal conductivity of copper and calculation of the heat transfer by the voltage measurement wires.

Temperature [K]	k, Thermal Conductivity [W/mK]	k*(T2-T1)	
1	4220	4220	:B3*(A4-A3)
2	8400	8400	
3	12500	12500	
4	16200	16200	
5	19500	19500	
6	22200	22200	
7	23900	23900	
8	24800	24800	
9	24900	24900	
10	24300	121500	
15	17100	85500	
20	10800	108000	
30	4450	44500	
40	2170	21700	
50	1250	12500	
60	829	8290	
70	647	6470	
80	557	5570	
90	508	5080	
100	482	24100	
150	429	21450	
200	413	20650	
250	406	20300	
300	401	20050	
350	396	19800	
400	393	39300	
500	386	38600	
600	379	75800	
800	366	73200	
1000	352	70400	
1200	339		

Diameter of wire [m]	0,0005	
A, Area [m^2]	1,9635E-07	
L, Length [m]	2	
Number of wires	34	
TH	300	
TL	20	
K*(TH-TL) [W/m]	318660	= SUM(C14:C26)
Thermal conductivity per wire [W]	0,031284372	
Thermal conductivity all wires [W]	1,06366866	

Thermal conductivity = k*A (TH-TL)/L

Appendix H

List of Equipment

Table H.1: List of Equipment

Experiment	Type	Function	Mark	Application
Assembly	WELLER WECP-20	Soldering iron	P02-0120	Pre-soldering
Assembly		Custom made soldering tool	None	Joining the Superconducters
Assembly and Testing the Field Winding	AGILENT 34970A	Data Logger	G05-0127	Data logger for voltage and temperature measurements
Assembly and Testing the Field Winding	AGILENT 34901A	Data Logger Module	G05-0183-01	Data logger module for voltage and temperature measurements
Testing the Field Winding	AGILENT 34901A	Data Logger Module	G05-0138-01	Data logger module for voltage and temperature measurements
Assembly and Testing the Field Winding	DELL Latitude D630	Computer	P07-1481	Collect data from data logger
Assembly and Testing the Field Winding	FLUKE 175	Multimeter	S03-0435	Measurments
Testing the Field Winding	ALCATEL 2015	Rotary Vane Pump	None	Pre-vacuum pump
Testing the Field Winding	PFEIFFER TPH200	Turbo Molecular High Vacuum Pump	None	Vacuum pump
Testing the Field Winding	PFEIFFER TCP200	Turbo Molecular Pump Controller	None	Controller and power supply for turbo molecualr pump
Testing the Field Winding	BALZERS PKG020	Pressure gauge	EFI P01-0051	Measuring pressure in cryostat
Testing the Field Winding	BALZERS TPG031A	Pressure gauge	None	Measuring pressure of vacuum pump
Testing the Field Winding	SUMITOMO CSW-71D	Compressor unit	S/N: 47D07334D	Compressor of the cryocooler
Testing the Field Winding	SUMITOMO RDK-408S	Cold Head	S/N: 3KS07062D	Cold Head of the Cryocooler
Testing the Field Winding	Agilent 6661A	System DC Power Supply	B02-0503	Power supply for the filed winding
Testing the Field Winding	LEYBOLD AF 16-25	Exhaust Filter for Vacuum Pumps	P05-0068	Exhaust filter
Testing the Field Winding	TENMA 72-2540	Power Supply	B02-0701	Current source for Cernox sensors